Geoscience Frontiers 15 (2024) 101775

Contents lists available at ScienceDirect

Geoscience Frontiers

journal homepage: www.elsevier.com/locate/gsf

Research Paper

Permian tectonic evolution and continental accretion in the eastern Central Asian Orogenic Belt: A perspective from the intrusive rocks

Anzong Fu [a,b], Hongyan Geng [c], Changzhou Deng [b,*], Chenglu Li [a], Jishuang Ding [a,d], Bizheng Yang [b], Wenpeng Yang [a]

[a] Heilongjiang Institute of Natural Resources Survey, Harbin 150036, China
[b] State Key Laboratory of Ore Deposit Geochemistry, Institute of Geochemistry, Chinese Academy of Sciences, Guiyang 550002, China
[c] Science Unit, Lingnan University, Hong Kong, China
[d] College of Earth Sciences, Jilin University, Changchun 130061, China

ARTICLE INFO

Article history:
Received 21 April 2023
Revised 2 October 2023
Accepted 22 December 2023
Available online 23 December 2023
Handling Editor: Sanghoon Kwon

Keywords:
Permian
Intrusive rocks
Eastern Central Asian Orogenic Belt
Paleo-Asian Ocean
Tectonic evolution

ABSTRACT

The tectonic evolution and history of continental accretion of the eastern Central Asian Orogenic Belt (CAOB) are not yet fully understood. In this study, we investigate Permian intrusive rocks from the Jiamusi Block of the eastern CAOB to constrain the tectonic evolution and continental accretion of this region during the late-stage evolution of the Paleo-Asian Ocean. Our new data show that Early Permian gabbro-diorites were derived from the partial melting of depleted mantle metasomatized by oceanic-slab-released fluids. Middle Permian adakitic granites have low Na_2O and MgO and high K_2O contents, indicating a thickened-lower-crust source. Late Permian S-type granites were derived from the partial melting of continental crust. A compilation of the available geochronological data for Permian intrusive rocks (including adakitic and A-, S-, and I-type granites and mafic rocks) from the eastern CAOB reveals that the A-type granites formed mainly during the Early–Middle Permian, S-type and adakitic granites mostly during the Middle–Late Permian, and I-type granites and mantle-derived mafic rocks throughout the Permian. The A-type granites, which are proposed to have been sourced from thinned continental crust, indicate an extensional setting in the eastern CAOB during the Early Permian. The Middle–Late Permian adakitic granites imply a thickened continental crust, which indicates a compressional setting. Therefore, the eastern CAOB underwent a transition from extension to compression during the Middle Permian, which was probably triggered by the late-stage subduction of Paleo-Asian oceanic crust. Considering the petrogenesis of the intrusive rocks and inferred regional tectonic evolution of the eastern CAOB, we propose that vertical underplating of mantle- and oceanic-slab-derived magmas contributed the materials for continental crust accretion.

1. Introduction

The N–E-trending giant Central Asian Orogenic Belt (CAOB) is located at the intersection of the Siberia, Tarim, and North China cratons. The tectonic evolution of this composite belt during the Phanerozoic has involved multi-stage oceanic slab subduction, large-scale crust–mantle interaction, and extensive magmatic activity (Sengör et al., 1993; Jahn, 2004; Windley et al., 2007; Wu et al., 2011; Xu et al., 2013, 2020; Wilde, 2015; Xiao et al., 2015; Konopelko et al., 2019). Therefore, reconstruction of the paleo-tectonic processes of the CAOB continues to be an important topic of scientific research with respect to geochemistry, petrology, tectonics, and economic geology. Within the prolonged tectonic history of the CAOB, the Permian has been regarded as a key period for understanding the evolution of the belt, as the Paleo-Asian Ocean gradually closed during this interval (Xiao et al., 2015; Song et al., 2018), leading to a protracted period of aggregation and cratonization (Chen et al., 2000; Zhu et al., 2022). The widely distributed Paleozoic strata and magmatic rocks in the CAOB and northern North China Craton (NCC) are important for understanding the tectonics of the Paleo-Asian Ocean basin and surrounding areas (Xiao et al., 2003; Chen et al., 2009; Wu et al., 2011; Safonova and Santosh, 2014; Wilde, 2015; Xu et al., 2020). Permian igneous rocks in the eastern CAOB are particularly useful for reconstructing the Permian geodynamic setting in this region (e.g., Song

* Corresponding author.
E-mail address: dengchangzhou@mail.gyig.ac.cn (C. Deng).

https://doi.org/10.1016/j.gsf.2023.101775

et al., 2018; Tang et al., 2020; Zhang and Jiang, 2021). Some key geological processes of the eastern CAOB, such as regional stress evolution and continental crust accretion, remain poorly understood.

Adakitic and S-, A-, and I-type granites are regarded as reliable indicators of tectonic setting, as these rocks are formed under specific geological conditions (Defant and Drummond, 1990; Sylvester, 1998; Broska et al., 2004). For example, adakitic granites are inferred to be generated by the partial melting of oceanic crust (Defant and Drummond, 1990; Sajona et al., 2000; Konopelko et al., 2021) or of thickened or delaminated lower continental crust (Atherton and Petford, 1993), or by the fractionation of mantle melts (Castillo et al., 1999; Kang et al., 2009). In contrast, S-type granites are generally formed by partial melting of Al-rich crustal materials under thermally anomalous conditions (Chappell and White, 1974; Barbarin, 1996; Sylvester, 1998; Jiang et al., 2013). A-type granites are generally formed in extensional tectonic settings by partial melting of thinned continental crust (Whalen et al., 1987; Maniar and Piccoli, 1989; Eby, 1992; Li et al., 2002; Wu et al., 2002), whereas I-type granites are commonly derived from partial melting of basaltic lower crust (Wu et al., 2011).

Igneous rocks with different magmatic sources are widely distributed in the eastern CAOB (Wu et al., 2011; Xu et al., 2013; Deng et al., 2019, 2022; Ding et al., 2022). Numerous geochemical and isotopic data have been reported for Permian igneous rocks from the eastern CAOB (e.g., Cao et al., 2013; Wang et al., 2015; Yang et al., 2015a; Cong et al., 2016; Li et al., 2022; Luan et al., 2022); however, a systematic study of Permian adakitic and S-, A-, and I-type granites and mantle-derived mafic rocks in this region has not yet been conducted. This has hindered the understanding of the tectonic evolution and continental accretion of the eastern CAOB.

This paper reports an integrated set of new geochemical, geochronological, and Hf isotopic data on S-type and adakitic granites and mantle-derived mafic rocks from the Jiamusi Block of the eastern CAOB. Integrated results of this study and compiled data for Permian intrusive rocks from the Songnen, Xing'an, and Jiamusi blocks and adjacent areas of the northern NCC are used as a basis on which to infer the Permian tectonic evolution and continental accretion history of the eastern CAOB.

2. Geological setting and samples

The eastern CAOB consists of several microblocks, namely, the Erguna, Xing'an, Songnen, and Jiamusi blocks, from northwest to southeast (Fig. 1a; Jahn, 2004; Sorokin et al., 2017; Wu et al., 2011). Owing to its unique geographical position, the eastern CAOB has been influenced by the Paleo-Asian Ocean (Sengör et al., 1993; Chen et al., 2000; Wu et al., 2011), Mongol–Okhotsk Ocean (Zorin, 1999; Nokleberg et al., 2000; Kelty et al., 2008; Metelkin et al., 2010; Yang et al., 2015b), and Paleo-Pacific Ocean (Xu et al., 2013) domains during the Phanerozoic. Each of these multiple domains was characterized by extensive magmatic activity and the large-scale convergence of various microblocks and arcs (Fig. 1b). The Jiamusi Block, which is also known as the Jiamusi–Xingkai–Bureya Massif (Zhou et al., 2010; Wilde et al., 2010; Wilde et al., 2015), is situated in the easternmost CAOB (Wilde et al., 1997, 2000; Zhou et al., 2010), adjacent to the Songnen Block to the northwest. The Jiamusi Block consists predominantly of Precambrian metamorphic basement (including the Mashan and Xingdong groups and the Heilongjiang Complex) and Paleo-Mesozoic sedimentary cover rocks (Fig. 2a; Li et al., 2020b). The Mashan Group comprises high-grade metamorphic rocks, including granulite, gneiss, and marble, with a peak metamorphic age of ~563 Ma (Wu et al., 2007, 2011; Yang et al., 2017b). The Xingdong Group is composed of amphibolite-facies magnetite-bearing quartzite (Gao et al., 2020). The Heilongjiang Complex, which is distributed along the west margin of the Jiamusi Block, consists of a suite of tectonic mélange and underwent high-pressure metamorphism at 185–165 Ma (Wu et al., 2007; Li et al., 2011; Zhao and Zhang, 2011, Dong et al., 2019). Paleo-Mesozoic sedimentary cover rocks, which are distributed mostly in the eastern margin of the Jiamusi Block, consist of Lower Devonian–lower Carboniferous marine and marine–continental transitional sedimentary and volcanic rocks (Zhou et al., 2018; Li et al., 2020b). Igneous rocks in the Jiamusi Block are composed mainly of Paleozoic intrusive rocks and late Mesozoic intrusive and volcanic rocks (Fig. 2a). Paleozoic intrusive rocks comprise Cambrian–Ordovician granitoids, including monzogranites, granodiorites, syenogranites, and garnet-bearing granites (Fig. 2b; Ren et al., 2012; Bi et al., 2014), as well as Late Carboniferous–Permian mantle-derived mafic rocks and granites (Wu et al., 2011; Bi et al., 2016; Dong et al., 2017a; Wutiepu et al., 2018; Bai et al., 2021; Zhu et al., 2022). The late Mesozoic igneous rocks include Early Cretaceous gabbro, dolerite, diorite, granodiorite, andesites, and rhyolites (Fig. 2c; Zhang et al., 2009; Yu et al., 2013a; Yin et al., 2019; Ding et al., 2022).

Samples of Permian gabbro-diorite investigated in this study were collected from the eastern Jiamusi Block (Fig. 2b). The medium- to fine-grained gabbro-diorites are composed mainly of plagioclase (40%–50%), clinopyroxene (35%–45%), hornblende (10%–15%) (Fig. 3a–d), and opaque minerals (5%; e.g., magnetite and pyrite), with minor accessory minerals (mainly apatite). Samples of Permian granitoids, including medium-grained muscovite granites and fine- to medium-grained granodiorites, were collected from the western margin of the Jiamusi Block (Fig. 2). The medium-grained muscovite granites are composed of K-feldspar (40%–45%), quartz (25%–30%), plagioclase (30%–35%), muscovite (1%–3%), and biotite (1%–3%) (Fig. 3e–g), with minor accessory zircon and apatite. The granodiorites occur as laccoliths and are intruded by the muscovite granite and Late Permian monzogranite (Fig. 2b). These granodiorites consist of plagioclase (45%–50%), quartz (20%–25%), K-feldspar (15%–20%), and biotite (5%–10%) (Fig. 3h and i), with minor accessory minerals (1%), including zircon, apatite, and magnetite.

3. Analytical methods

3.1. Zircon U–Pb dating

Samples of two gabbro-diorites (samples USS-1 and USS-2), one granodiorite (Pm106-U-Pb), and two muscovite granites (Pm102-U-Pb and Pm103-U-Pb) were collected for zircon U–Pb dating. Zircon grains were handpicked under a binocular microscope, mounted in epoxy disks, and polished at Guangzhou Tuoyan Analytical Technology, Guangzhou, China. After obtaining cathodoluminescence (CL) images, zircon U–Pb dating was performed using laser ablation–inductively coupled plasma–mass spectrometry (LA-ICP-MS) at Wuhan Sample Solution Analytical Technology (WSSATCL), Wuhan, China. Laser sampling was performed using a GeolasPro LA system. An Agilent 7700e ICP-MS instrument was used to acquire ion-signal intensities. Time-dependent drifts of U–Th–Pb isotopic ratios were corrected using linear interpolation (with time) for every 5–10 analyses (Liu et al., 2010). Concordia diagrams were created and weighted-mean ages calculated using Isoplot/Ex_ver3 (Ludwig, 2003). The zircon standard Plesovice was dated as an unknown sample and yielded a weighted-mean $^{206}Pb/^{238}U$ age of 338 ± 1 Ma (2SD, n = 12), which is identical within analytical uncertainties to the recommended $^{206}Pb/^{238}U$ age of 337.13 ± 0.37 Ma (2SD) (Sláma et al., 2008).

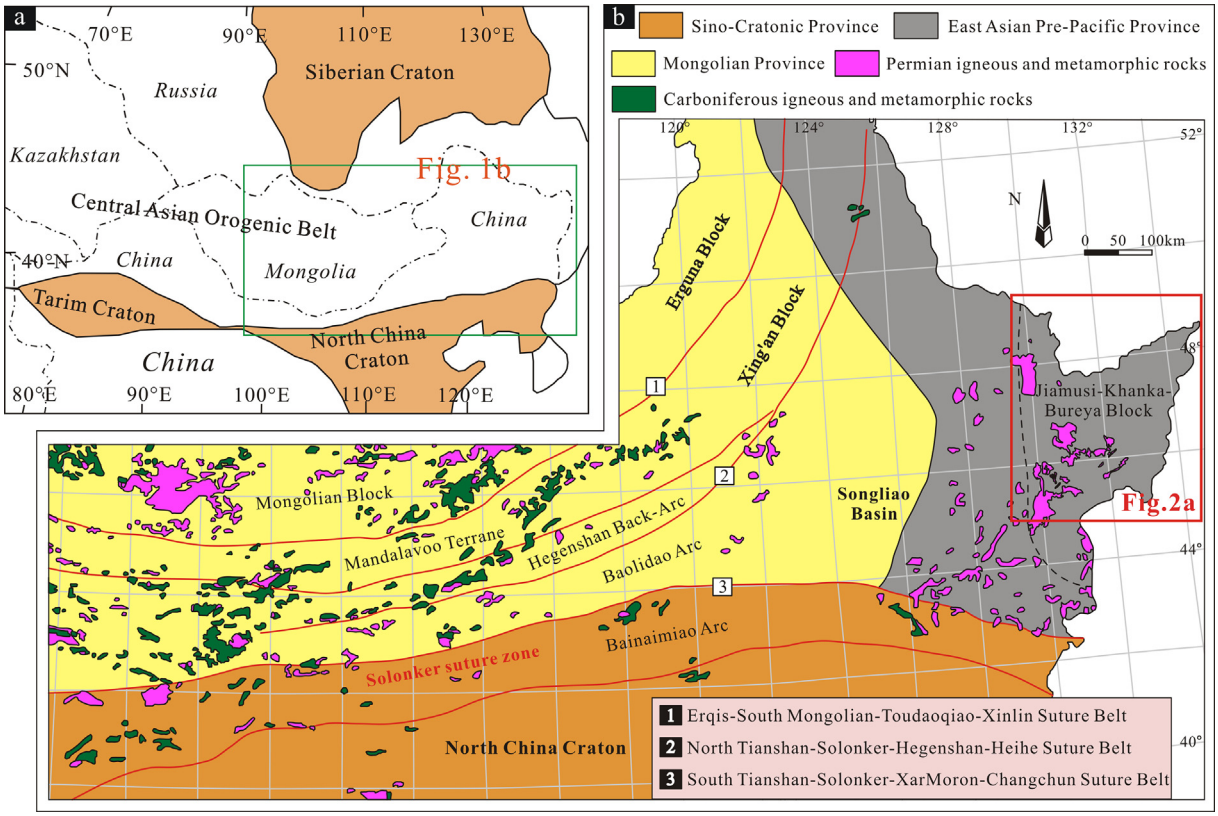

Fig. 1. (a) Tectonic sketch map of the CAOB (after Jahn, 2004); (b) simplified geological map of the eastern CAOB, showing the distribution of Permian igneous rocks (after Eizenhöfer and Zhao, 2018; Jing et al., 2022).

3.2. Whole-rock major- and trace-element compositions

Ten gabbro-diorite, six granodiorite, and six muscovite granite samples were collected for whole-rock geochemical analysis at Wuhan Sample Solution Analytical Technology, Wuhan, China. Major-element contents were measured using X-ray fluorescence spectrometry involving analysis of fused glass disks with lithium borate. Trace-element contents were measured using ICP-MS. The analytical methods and procedures followed those described by Gao et al. (2002). The analytical uncertainties for major- and trace-element contents are better than 1% and 10%, respectively.

3.3. In situ zircon Hf isotope analyses

In situ zircon Hf isotope analyses were performed at Wuhan Sample Solution Analytical Technology, Wuhan, China, using a Neptune multi-collector (MC)-ICP-MS instrument equipped with a 193 nm laser. All zircon grains were analyzed using a single-spot ablation mode with a spot size of 35 μm. Zircon standard GJ-1 was used for external standardization and yielded a weighted-mean value of 0.282014 ± 0.000007 (2σ, n = 6). Analytical methods and procedures followed those reported by Wu et al. (2006).

4. Results

4.1. Zircon U–Pb dating

Zircons grains from the gabbro-diorite (USS-1 and USS-2), granodiorite (Pm106U-Pb), and muscovite granite (Pm102U-Pb and Pm103U-Pb) are euhedral to subhedral in shape and have lengths of 35–300 μm. The zircons have well-developed oscillatory zoning (Fig. 4a) and high Th/U ratios of 0.06–0.97 (with only three values of < 0.1; Supplementary Data Table S1), indicating an igneous origin (Koschek, 1993).

The two gabbro-diorite samples yield weighted-mean $^{206}Pb/^{238}U$ ages of 273 ± 2 Ma (MSWD = 0.54; n = 24) and 276 ± 2 Ma (MSWD = 1.14; n = 25), respectively (Fig. 4b and c).

The granodiorite sample yielded two groups of ages, with 3 older zircon grains yielding $^{206}Pb/^{238}U$ ages of 418–286 Ma and the other 13 younger grains yielding a weighted-mean $^{206}Pb/^{238}U$ age of 265 ± 2 Ma (MSWD = 0.66; n = 13; Fig. 4d).

The two muscovite granite samples yielded weighted-mean $^{206}Pb/^{238}U$ ages of 254 ± 1 Ma (MSWD = 0.47; n = 23) and 258 ± 1 Ma (MSWD = 0.83; n = 21) (Fig. 4e and f), respectively, whereas three inherited zircons gave $^{206}Pb/^{238}U$ ages of 541–306 Ma (Supplementary Data Table S1).

4.2. Whole-rock geochemistry

Whole-rock geochemical data from this study, together with previously published data, are presented in Figs. 5 and 6. The 276–273 Ma gabbro-diorite samples have SiO_2 contents of 51.01–57.93 wt.%, MgO contents of 3.14–6.66 wt.%, and total Fe_2O_3 ($Fe_2O_3^T$) contents of 6.58–8.70 wt.% (Supplementary Data Table S2), falling in the sub-alkaline series in a diagram of K_2O vs. SiO_2 (Fig. 5c). The samples display slight enrichment in light rare earth elements (LREEs) [$(La/Yb)_N$ = 3.24–10.54], with negligible to positive Eu anomalies (Eu/Eu^* = 0.89–1.58) (Fig. 6a). A primitive-mantle-normalized trace-element spidergram shows that all of these rocks are enriched in Ba, Th, K, Pb, Sr, and LREEs and depleted in Nb, Ta, P, Ti, and heavy REEs (HREEs; Fig. 6b).

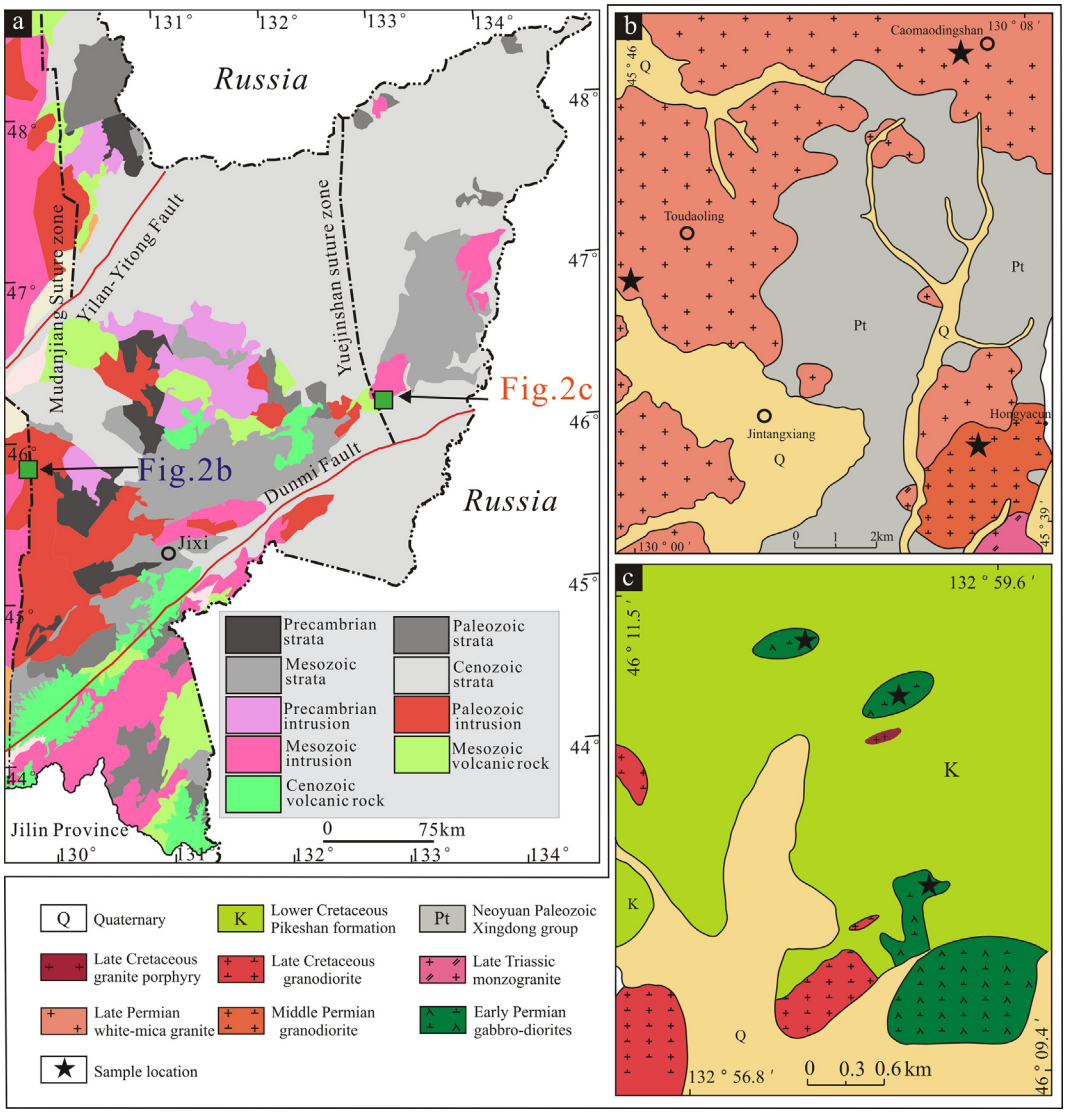

Fig. 2. (a) Simplified geological map of the Jiamusi Block (after Wu et al., 2011; Xu et al., 2013); (b) geological map of the Jiangtang area, showing the locations of the adakitic and S-type igneous rocks investigated in this study; (c) geological map of the Dongfanghong area, showing the locations of mafic rocks investigated in this study.

The 265 Ma granodiorite samples display limited variation in SiO_2 contents (64.62–68.98 wt.%; Fig. 5a), with high CaO (2.11–2.91 wt.%) and Al_2O_3 (15.52–18.2 wt.%) contents and low MgO contents (0.86–1.33 wt.%) and Mg# values (37–44). The granodiorite samples have A/CNK ratios of 1.13–1.21, indicating a weakly peraluminous nature (Fig. 5b), and fall in the high-K calc-alkaline series (Fig. 5c). Trace-element data reveal that the granodiorites are enriched in LREEs, Rb, K, Pb and Ba and depleted in HREEs [$(La/Yb)_N$ = 14.4–31.69], Nb, Ta, Ti, and P, with negative Eu anomalies (Eu/Eu* = 0.62–0.90) (Fig. 6c and d). The granodiorite samples have high K_2O (3.67–4.30 wt.%; Fig. 7a) and Sr (445–542 ppm) contents, high K_2O/Na_2O ratios (>0.75; Fig. 7b), and low Yb (1.00–1.69 ppm) and Y (14.14–18.27 ppm) contents, showing affinity to adakites (Fig. 7c and d).

The 258–254 Ma muscovite granite samples have high SiO_2 (70.40–72.72 wt.%), Na_2O + K_2O (6.96–8.86 wt.%), and Al_2O_3 (14.30–15.27 wt.%) contents and low TiO_2 (0.07–0.30 wt.%), MgO (0.09–0.49 wt.%), CaO (0.26–1.69 wt.%), and P_2O_5 (0.01–0.21 wt.%) contents. The rocks are characterized by low Mg# values (9–29) and high A/CNK ratios (1.13–1.24) and plot in the peraluminous area in an A/CNK vs. A/NK diagram (Fig. 5b). The muscovite granites show marked enrichment in LREEs and slight negative Eu anomalies (Eu/Eu* = 0.62–0.92). Trace-element data reveal enrichment of these rocks in Rb, Ba, K, and Pb and depletion in Nb, Ta, Ti, Zr, and P (Fig. 6e and f).

4.3. Zircon Hf isotopes

Zircon grains from the gabbro-diorites have initial $^{176}Hf/^{177}Hf$ ratios of 0.282732–0.282842 and $\varepsilon_{Hf}(t)$ values of 4.30–8.35, with corresponding one-stage model ages of 741–573 Ma, plotting between the chondrite and depleted-mantle evolution lines in an $\varepsilon_{Hf}(t)$–age diagram (Fig. 8). Zircon grains from the granodiorite and muscovite granites have initial $^{176}Hf/^{177}Hf$ ratios of 0.282337–0.282485 and 0.282285–0.282635, respectively, with $\varepsilon_{Hf}(t)$ values of −9.73 to −4.36 and −11.71 to 0.50, respectively (Fig. 8), and corresponding two-stage model ages of 1904–1568 and 2025–1251 Ma, respectively (Supplementary Data Table S3).

Fig. 3. Photographs and photomicrographs of igneous rocks of the eastern Central Asian Orogenic Belt. (a, b) Medium-grained gabbro-diorite; (c, d) fine-grained gabbro-diorite; (e–g) muscovite granite; (h, i) medium-grained granodiorite. Abbreviations: Pl, plagioclase; Q, quartz; Bi, biotite; Kf, K-feldspar; Hb, hornblende.

5. Discussion

5.1. Multiple sources of the studied Jiamusi Block Permian igneous rocks

5.1.1. Early Permian gabbro-diorites: Metasomatized mantle source

The Early Permian gabbro-diorites have low SiO_2 (51.00–57.93 wt.%) and high MgO (3.14–6.66 wt.%) and $Fe_2O_3^T$ (6.58–8.70 wt.%) contents and Mg# values (49–65), indicating a mantle-dominated source. These rocks have Rb/Sr ratios of 0.01–0.05 (mean = 0.03), Zr/Hf ratios of 33.8–40.8 (mean = 37.7), and Nb/Ta ratios of 11.6–18.4 (mean = 15.9), similar to those of primitive mantle (0.03, 37, and 17.8, respectively; Sun and McDonough, 1989; McDonough and Sun, 1995). The gabbro-diorites show enrichment in large-ion lithophile elements, Ba, Pb, Sr, and LREEs (Fig. 6), resembling igneous rocks that originate from metasomatized mantle (Pearce, 1983). Their $\varepsilon_{Hf}(t)$ values (+4.35 to + 8.35) are lower than those of depleted mantle (Fig. 8), indicating the involvement of enriched materials from the crust in the source. Their negative Nb and Ta anomalies, low Nb/La ratios (0.30–0.41, mean = 0.34), high Rb/Y, Th/Zr and Ba/Th ratios, and slightly variable Nb/Y, Nb/Zr, and La/Sm ratios indicate that the gabbro-diorites were derived from depleted mantle metasomatized by oceanic-slab-derived fluids (e.g., Stern, 2002; Kessel et al., 2005; Fig. 9). Batch melting modeling shows that the gabbro-diorites were probably generated by partial (2.5%–7%) melting of a 2% spinel-bearing lherzolite source (Fig. 10a). The presence of spinel suggests that the partial melting occurred at low pressure (corresponding to 75–85 km depth; Sajona et al., 1996). The high Ta/Yb and Th/Yb ratios of the studied rocks are consistent with their formation in an active-continental-margin setting (Fig. 10b; Pearce, 1983). In summary, the gabbro-diorites were sourced from metasomatized mantle in an active continental margin setting.

5.1.2. Middle Permian adakitic granites: Thickened-continental-crust source

The Middle Permian granodiorites have high SiO_2 (64.62–68.98 wt.%), Al_2O_3 (15.52–18.20 wt.%), and Sr (445–542 ppm) contents, low Y (14.14–18.27 ppm) and Yb (1–1.69 ppm) contents, and high Sr/Y (25.3–37.9) and La/Yb (20.1–44.2) ratios, thereby showing adakitic affinity (Fig. 7; Defant and Drummond, 1990). Different models have been proposed for the genesis of adakitic rocks, including the partial melting of subducting oceanic slab (Defant and Drummond, 1990; Sajona et al., 2000), mixing of felsic and mafic magmas (Guo et al., 2007; Streck et al., 2007), fractional crystallization or assimilation of mantle melts (Castillo et al., 1999; Kang et al., 2009), and partial melting of delaminated lower crust (Xu et al., 2002; Wang et al., 2004) or thickened lower crust (Atherton and Petford, 1993).

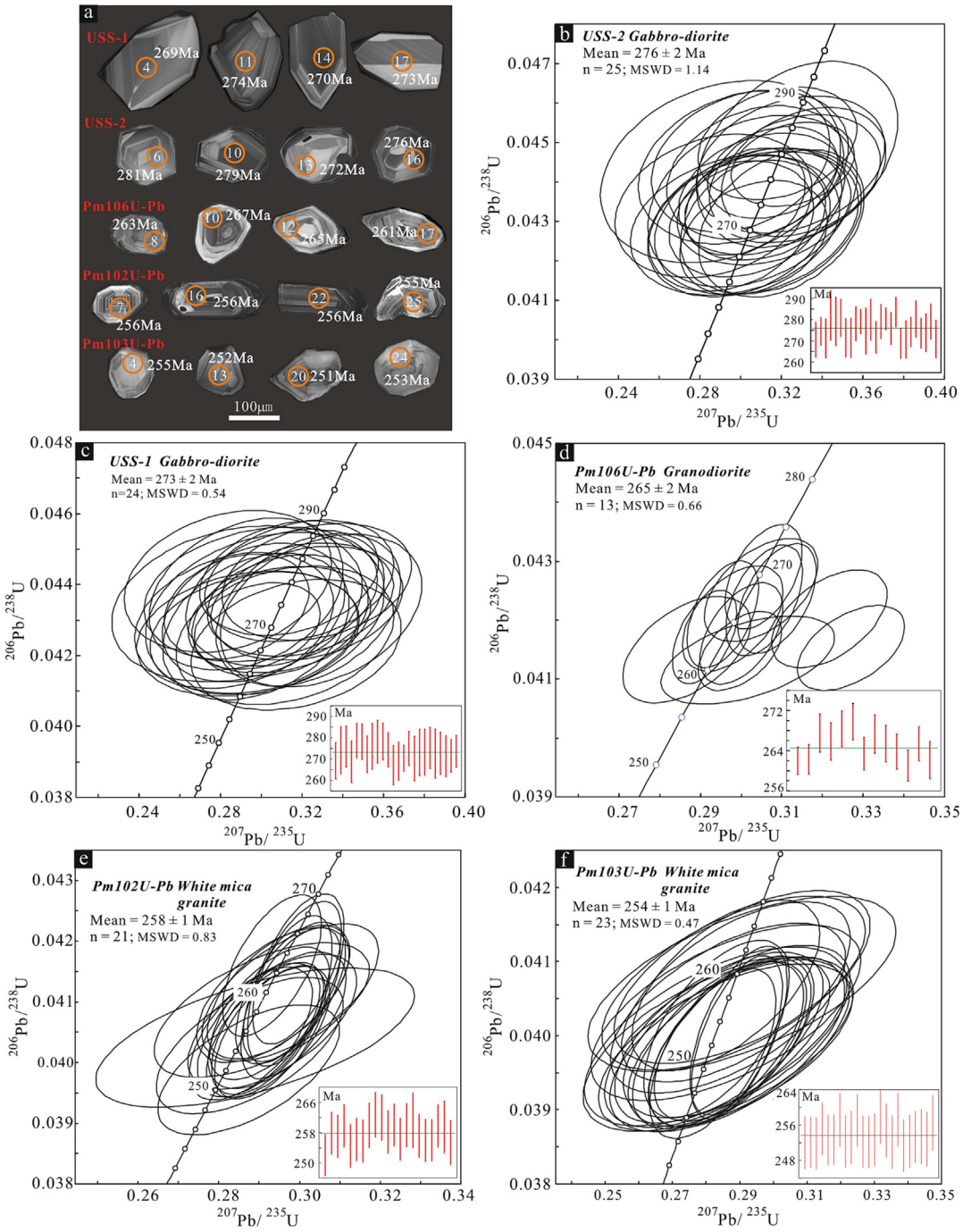

Fig. 4. (a) Cathodoluminescence images of representative zircons analyzed for U-Pb isotope dating. (b–f) Concordia diagrams for U–Pb ages of zircons from the studied igneous rocks.

The studied granodiorites have Na_2O contents of 3.07–4.00 wt.% and Na_2O/K_2O ratios of 0.71–1.07, which are lower than those generated by the partial melting of subducting oceanic crust (Na_2O content of 4.88 wt.% and Na_2O/K_2O ratios of 2.5–6.5; Sajona et al., 2000), thereby precluding an oceanic-crust source. Adakitic rocks formed by the mixing of felsic and mafic magmas typically show wide variation in SiO_2 and high MgO and Cr contents and contain mafic xenoliths in intrusions (Guo et al., 2007; Streck et al., 2007). However, the granodiorite samples exhibit limited variation in SiO_2 contents (64.62–68.98 wt.%), have low MgO (0.86–1.33 wt.%) and Cr (8.01–12.19 ppm) contents, and lack mafic xenoliths and voluminous coeval mafic rocks, precluding the mixing of crustal and mafic magmas. The granodiorites have Rb/Sr and Nb/Ta ratios of 0.27–0.36 (mean 0.31) and 9.24–12.70 (mean 11.66), respectively, similar to those of granodiorites sourced from the crust (Rb/Sr = 0.35 and Nb/Ta = 11.4; Taylor and McLennan, 1985) but different from those sourced from the mantle (Rb/Sr = 0.03; Sun and McDonough, 1989; Nb/Ta = 17.8, McDonough and Sun, 1995). Therefore, the studied adakitic granodiorites were likely formed by the partial melting of crustal materials. Previous studies have proposed that adakitic rocks sourced from delaminated continental crust have high MgO (>2 wt.%), Cr (>20 ppm), Ni (>10 ppm), and V (>85 ppm) contents and K/Rb ratios (generally > 350) (Wang et al., 2004; Fu et al., 2022). However,

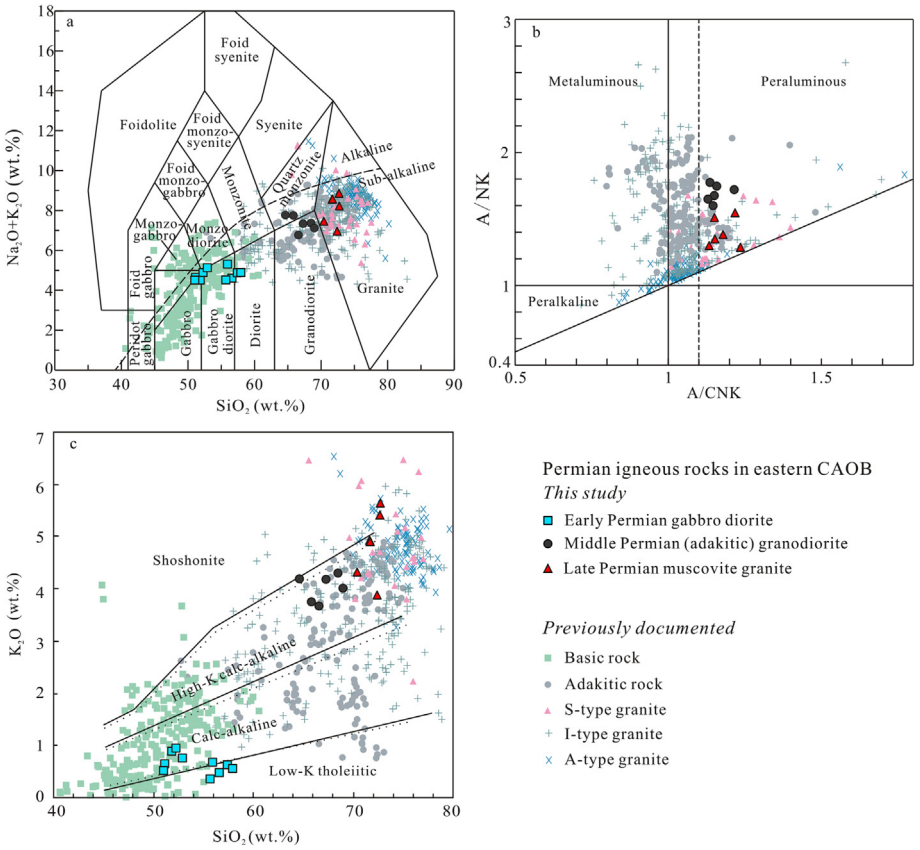

Fig. 5. Diagrams of (a) ($Na_2O + K_2O$) vs. SiO_2 (after Irvine and Baragar, 1971), (b) A/NK vs. A/CNK (after Maniar and Piccoli, 1989), and (c) K_2O vs. SiO_2 (Peccerillo and Taylor, 1976) for Permian igneous rocks from the eastern CAOB. A/NK = Al/(Na + K) (molar ratio); A/CNK = Al/(Ca + Na + K) (molar ratio). Geochemical data from previous studies are listed in Supplementary Data Table S4.

the granodiorite samples of this study show low MgO (0.86–1.33 wt.%) and Cr (8.01–12.19 ppm) contents and low K/Rb ratios (214–234), which instead indicate a thickened-lower-crust source. In addition, the granodiorite samples plot in the field of thickened lower crust in the discrimination diagrams of Fig. 11. These rocks also show negative $\varepsilon_{Hf}(t)$ values ranging from −9.7 to −4.4, with two-stage Hf model ages of 1904–1568 Ma, indicating the involvement of ancient basement materials in the source.

5.1.3. Late Permian S-type granites: Paleo-crustal sedimentary source

The Late Permian muscovite granites are characterized by high SiO_2 (70.40–72.72 wt.%) and Al_2O_3 (14.30–15.27 wt.%) contents, low CaO (mean = 1.05 wt.%) and MgO (mean = 0.29 wt.%) contents, and high A/CNK (1.13–1.24) and Na_2O/K_2O ratios (mean = 0.69). These rocks have corundum contents (standard molecular contents) of 1.81–2.90 wt.% (mean = 2.41 wt.%) and other similar geochemical characteristics to those of peraluminous S-type granitoids (Ma, 1992; Sylvester, 1998; Liao et al., 2006). Previous studies have revealed that S-type granites generally show a positive correlation between P_2O_5 and SiO_2 contents and negative correlations between La and SiO_2 contents and between Th or Y contents and Rb content (e.g., Chappell, 1999). The studied muscovite granites exhibit similar geochemical characteristics to those of S-type granites in diagrams of P_2O_5 vs. SiO_2, La vs. SiO_2, Th vs. Rb, and Y vs. Rb (Fig. 12).

Strongly peraluminous S-type granites are typically formed by the partial melting of crustal Al-rich sediments (Sylvester, 1998). In this study, the muscovite granite samples plot in the greywacke field (Fig. 13a) or in the area of overlap between the greywacke and pelite fields (Fig. 13b). Therefore, we conclude that the source of the muscovite granites was dominated by pelite and greywacke materials.

The studied muscovite granites have low Sr (120–410 ppm, mean = 231.7 ppm), Yb (0.58–1.57 ppm, mean = 0.94 ppm), and Y (7.14–15.07 ppm, mean = 12.36 ppm) contents. The low Sr contents (<300 ppm) indicate the presence of plagioclase in the residual source, and the low Yb (<1.9 ppm) and Y (<15 ppm) contents suggest the presence of garnet in the residual source (Castillo, 2006). The coexistence of plagioclase and garnet in the residual source indicates that partial melting occurred at pressures of 0.5–1.2 GPa (Patiño Douce, 2005). The zircon saturation thermometer proposed by Miller et al. (2003) yields a crystallization temperature of 736–820 °C (mean = 774 °C) for the muscovite granites, which is within the range of the muscovite dehydration temperature (Harris et al., 1995; Weinberg and Hasalová, 2015). The muscovite granites show higher Rb/Sr ratios with decreasing Sr and Ba contents, indicating fractional crystallization of muscovite during magmatic evolution (Fig. 14; Inger and Harris, 1993).

5.2. Permian tectonic evolution of the eastern CAOB

The spatial–temporal distribution of magmatism and inferred tectonic evolution provide information about the kinematic processes involved in the formation of accretionary terranes; therefore, they give insights into plate tectonic settings. Our new results, combined with compiled geochronological data for Permian granites from the eastern CAOB, show that adakitic and S-type granites formed predominantly during the Middle–Late

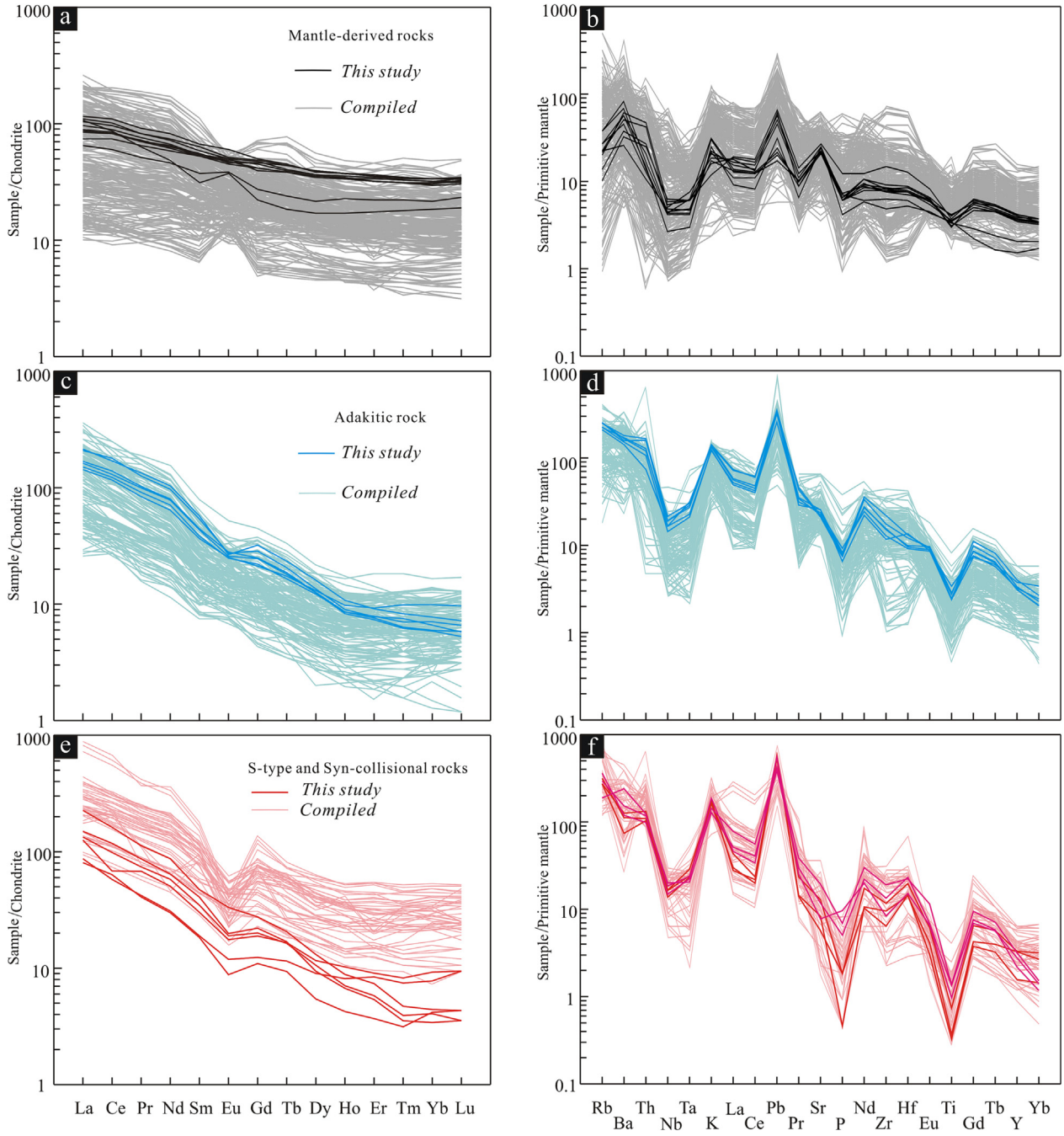

Fig. 6. Chondrite-normalized REE variation diagrams (a, c, and e) and primitive-mantle-normalized trace-element spider diagrams (b, d, and f) for Permian igneous rocks from the eastern CAOB. Normalization values are from Sun and McDonough (1989). Data sources are the same as in Fig. 5.

Permian (Figs. 15a, b and 16a), whereas A-type granites were generated mainly during the Early–Middle Permian (Figs. 15c and 16b). The temporal distribution of granites in the eastern CAOB implies that a transition in the regional stress occurred during the Permian. Previous studies have established that the initial westward subduction of the Paleo-Pacific slab beneath NE China occurred primarily during the early Mesozoic (Wu et al., 2011; Li et al., 2017; Xu et al., 2022). Therefore, Permian magmatism in the eastern CAOB was unlikely to have been dominated by the Paleo-Pacific Ocean tectonic domain. During the late Paleozoic–early Mesozoic (315–230 Ma), the Mongol–Okhotsk Ocean tectonic domain was initiated in the eastern margin of the Jiamusi–Khanka Block (Chen et al., 2023) and governed the tectonic evolution and crustal accretion of the eastern and northern CAOB (Zhou and Wilde, 2013). A recent study has concluded that the Paleo-Asian Ocean closed along the Solonker–Xarnoron–Changchun Suture within a divergent double-subduction regime at the end of the Permian (250 Ma), leading to the amalgamation of the Erguna–Xing'an–Songliao Block and the NCC (Chen et al., 2023), which implies that the Paleo-Asian Ocean existed between the eastern CAOB and the NCC during the Permian. Therefore, we infer that Permian magmatism in the northern NCC and southeastern CAOB was influenced mainly by the Paleo-Asian Ocean tectonic domain.

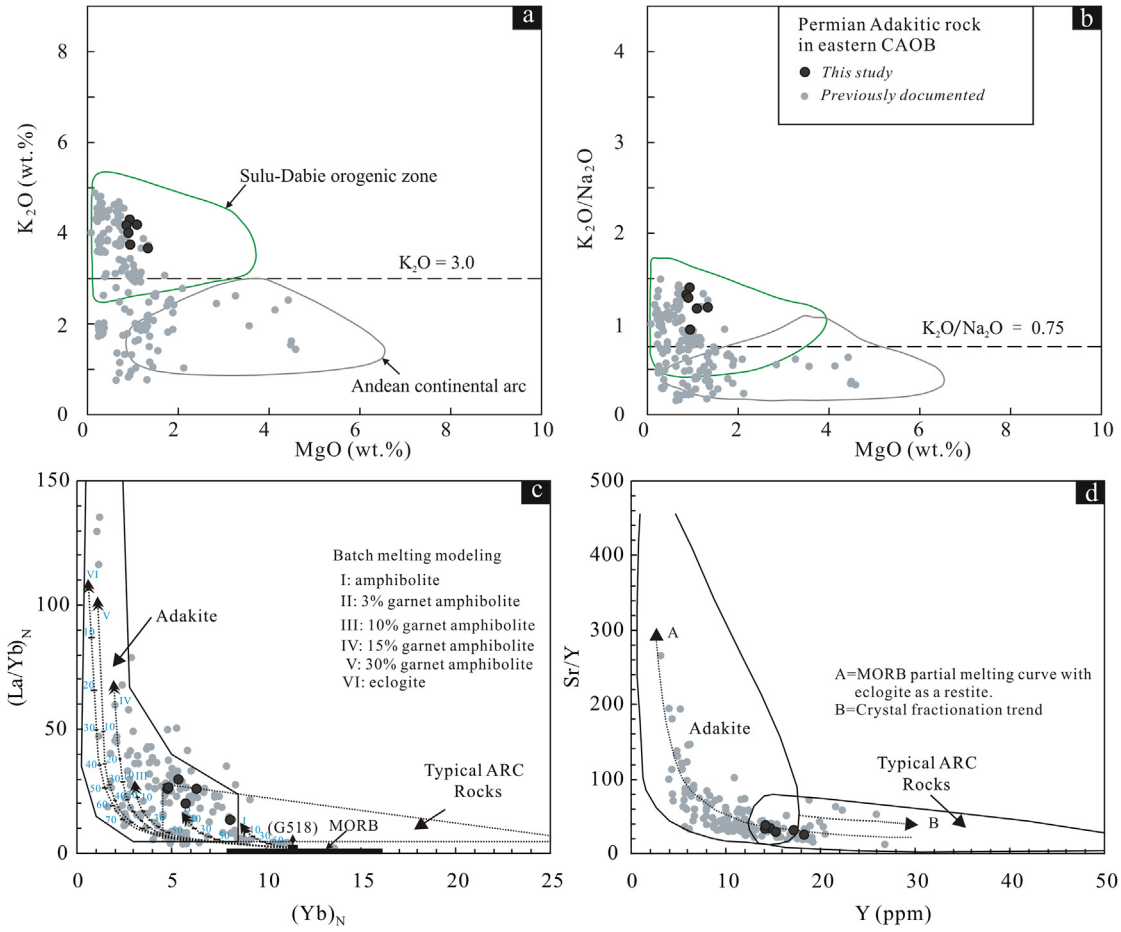

Fig. 7. Diagrams of (a, b) MgO vs. K_2O and MgO vs. K_2O/Na_2O (after Shen et al., 2021), (c) $(La/Yb)_N$ vs. $(Yb)_N$ (Drummond et al., 1996), and (d) Sr/Y vs. Y (after Defant and Drummond, 1990) for Permian adakitic rocks from the eastern CAOB. An Eastern Pontides gabbro (G518) (Dokuz et al., 2006) was used as the source rock for REE modeling under amphibolite and eclogite conditions, with varying garnet contents and respective partition coefficients (I–VI), where N means normalized to chondrite (Sun and McDonough, 1989). Data sources are the same as in Fig. 5.

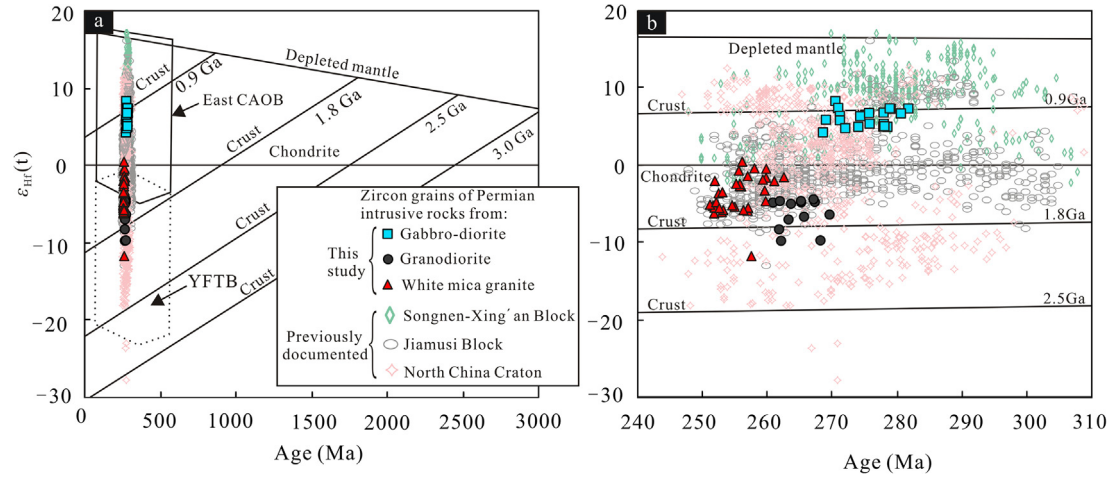

Fig. 8. Correlations between (a, b) Hf isotopic compositions and U-Pb ages of zircons from Permian igneous rocks in the eastern CAOB. The regions of the eastern CAOB and the Yanshan Fold and Thrust Belt (YFTB) are as defined by Yang et al. (2006). Compiled Hf isotopic data are listed in Supplementary Data Table S5.

The Early Permian A-type granites from the eastern CAOB were formed by the partial melting of juvenile basaltic lower crust (Yuan et al., 2016) in a back-arc (Wang et al., 2020c) or post-collisional (Tong et al., 2015; Wutiepu et al., 2018; Zhang et al., 2018b; Zhou et al., 2021) extensional setting. The Paleo-Asian Ocean between the Songnen and Xing'an blocks gradually narrowed and

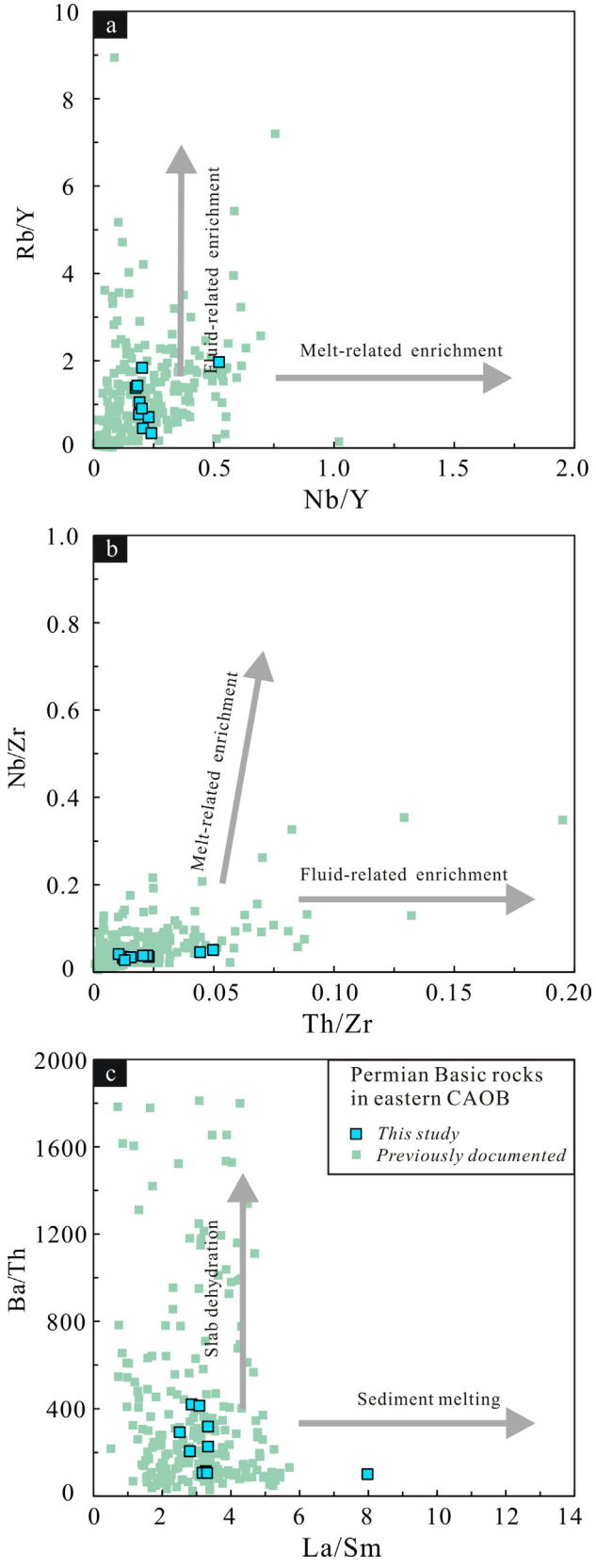

Fig. 9. Diagrams of (a, b) Rb/Y vs. Nb/Y, and Nb/Zr vs. Th/Zr (after Kepezhinskas et al., 1997) and (c) Ba/Th vs. La/Sm (after Labanieh et al., 2012) for Permian mafic rocks from the eastern CAOB. Data sources are the same as in Fig. 5.

closed during the Permian (Zhao et al., 2010; Tong et al., 2015; Ma et al., 2019; Xu et al., 2020). The Early Permian A-type granites distributed along the Heihe–Hegenshan suture zone were likely formed in a post-collisional extensional setting (Xu et al., 2020). The Early Permian A-type granites were formed in a back-arc extensional setting, probably as a result of rollback of the subducting Paleo-Asian oceanic slab and subsequent upwelling of asthenospheric material (Chai et al., 2020). Similarly, the Middle Permian A-type granites were also derived by the partial melting of lower crust in a back-arc (Bi et al., 2016) or post-collisional (Zhao et al., 2016) extensional setting associated with the evolution of the Paleo-Asian Ocean. In addition, the Early Permian Hahushuo pluton in the adjacent NCC is considered to have been emplaced in an extensional setting (Shi et al., 2019). These various lines of evidence together indicate that the eastern CAOB was under the influence of a regional extensional setting during the Early–Middle Permian (Fig. 17a), similar to the Early Permian extensional setting in the western CAOB (Konopelko et al., 2018). This conclusion is supported by the characteristics of Late Carboniferous–Middle Permian sedimentary rocks of the eastern CAOB (Zhang, 2013; Eizenhöfer et al., 2015; Zhang et al., 2018a, 2021; Li et al., 2019; Wang et al., 2020a; Ji et al., 2020). For example, the Late Carboniferous–Early Permian Shoushangou Formation in central Inner Mongolia is characterized by sandstone turbidites with a Bouma sequence and numerous tuffs in the lower part of the formation, which are consistent with deposition in a back-arc basin (Wang et al., 2020a). The Late Carboniferous–Early Permian Halatumiao Formation in the Erenhot area consists mainly of fine-grained blackish sedimentary rocks with a thickness of 6–7 km, indicating deep-ocean-basin conditions (Ji et al., 2020). The Middle Permian Zhesi Formation in the Solonker suture zone comprises conglomerate, sandstone, and interbedded mudstone and limestone, some layers of which contain Permian brachiopod fossils, indicating a back-arc basin sedimentary environment (Zhou et al., 2015). The characteristics of the Late Carboniferous–Middle Permian strata imply the opening of a back-arc basin under continuous extension in the eastern CAOB (Eizenhöfer et al., 2015; Zhou et al., 2015).

Early Permian igneous rocks with adakitic features (e.g., high Sr/Y ratios) are distributed sporadically in the northern margin of the NCC (e.g., the 275 Ma Dongshengmiao pluton; Hu et al., 2015a), and in the Songnen (e.g., the 291–289 Ma Xi Ujimqin adakitic rocks; Li et al., 2022) and Jiamusi (e.g., the 284 Ma Liulian pluton; Yu et al., 2013b) blocks (Fig. 16a). These adakitic rocks are regarded to have been formed by the partial melting of oceanic slab (e.g., Li et al., 2022) or by the mixing of mantle and crustal melts (e.g., Yu et al., 2013b; Hu et al., 2015a). In comparison, Middle-Late Permian adakitic rocks, which are widely distributed in the eastern CAOB (Fig. 16a), had multiple magma sources (Cao et al., 2013; Wang et al., 2015; Yang et al., 2015a; Cong et al., 2016; Luan et al., 2022). The 267 Ma Guangxingyuan tonalites in the northern margin of the NCC were produced by mixing of mantle and crustal melt (Zhao et al., 2016), and the 267 Ma adakitic granodiorites from the Huanan area in the Jiamusi Block were formed by partial melting of oceanic slab (Cong et al., 2016). However, most of the adakitic rocks (e.g., the 259 Ma Youyi, 260 Ma Zhaobeishan, 261 Ma Gongzhuling, and 272–261 Ma Bulitai–Dabusu plutons in the northern margin of the NCC; the 261 Ma Chunhua granodiorite in the Songnen Block; and the 267 Ma Hengtoushan pluton in the Jiamusi Block) were generated by the partial melting of thickened-crustal materials (Wang et al., 2015, 2020b; Li et al., 2020a; Bai et al., 2021; Hui et al., 2021; Yang et al., 2021; Luan et al., 2022). The above-mentioned features imply the existence of thickened continental crust in the eastern CAOB during the

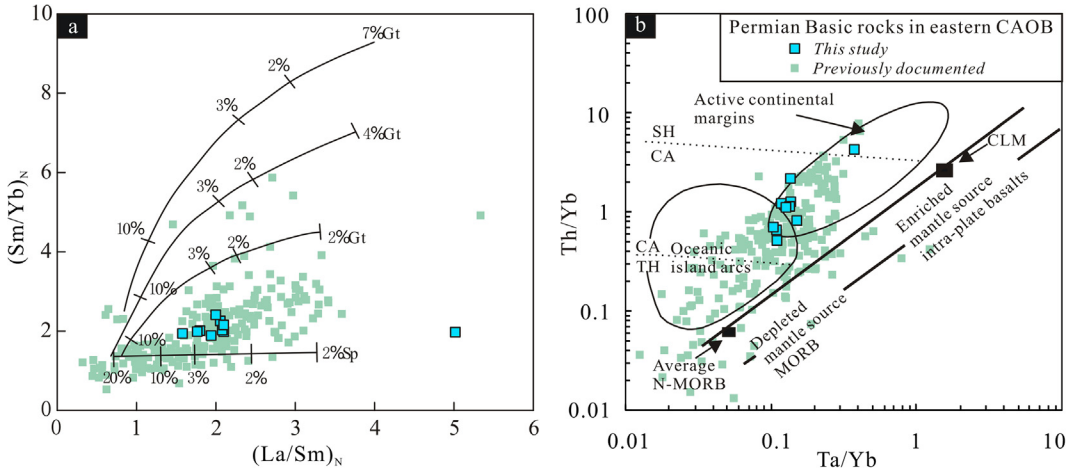

Fig. 10. Diagrams of (a) $(Sm/Yb)_N$ vs. (La/Sm) (after McKenzie and O'Nions, 1991) and (b) Th/Yb vs. Ta/Yb (after Pearce, 1982) for Permian mafic rocks from the eastern CAOB, where N means normalized to chondrite (Sun and McDonough, 1989). Data sources are the same as in Fig. 5.

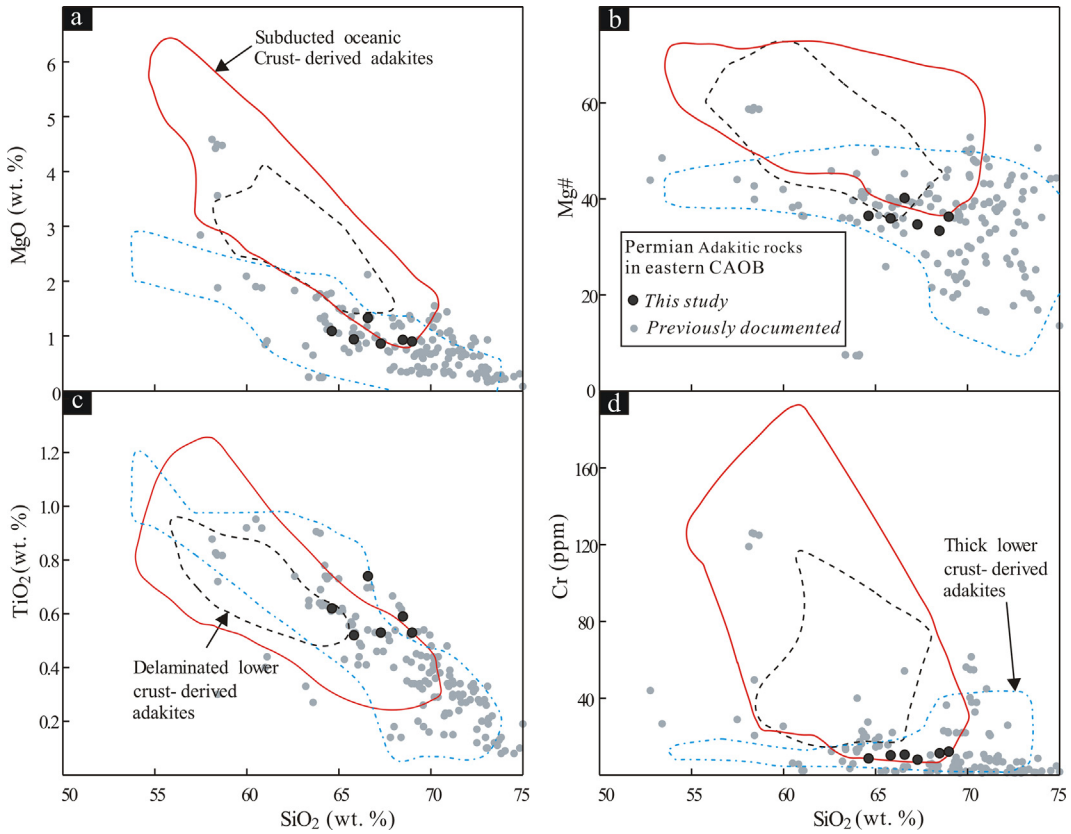

Fig. 11. Diagrams of (a) MgO, (b) Mg#, (c) TiO_2, (d) Cr vs. SiO_2 for adakitic granites from the eastern CAOB. Data sources are the same as in Fig. 5.

Middle–Late Permian. The existence of thickened continental crust is supported by the occurrence of coeval S-type granites in the eastern CAOB, such as Middle–Late Permian S-type granites in the northern margin of the NCC and the Songnen and Jiamusi blocks (Figs. 12 and 13; Cui et al., 2013; Wang et al., 2016; Zhang et al., 2017; Yang et al., 2017a). Although S-type granites can be formed in post-collisional (Sylvester, 1998; Hu et al., 2015b), syn-collisional (Barbarin, 1996; Jiang et al., 2013), or arc (Collins and Richards, 2008) settings, the appearance of coeval adakitic rocks sourced from thickened lower crust indicates a Middle–Late Permian orogenic setting in the eastern CAOB. This interpretation is supported by the results of thermochronological and regional metamorphic studies, which indicate collisional and metamorphic events in the eastern CAOB during the Middle–Late Permian (Wen et al., 2017; Li et al., 2010, 2021). The Middle–Late Permian orogeny in the eastern CAOB was likely associated with

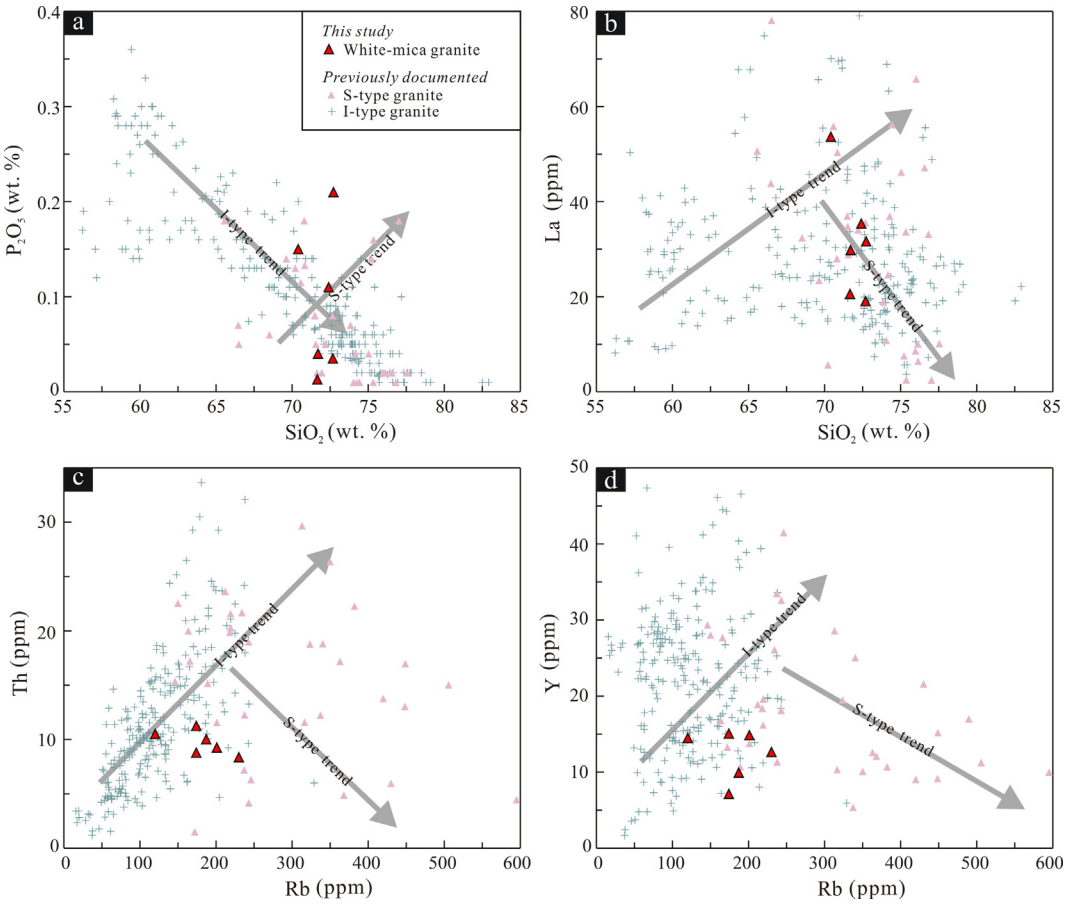

Fig. 12. Diagrams of (a) P_2O_5 vs. SiO_2, (b) La vs. SiO_2, (c) Th vs. Rb and (d) Y vs. Rb (Chappell, 1999) for I- and S-type granites from the eastern CAOB. Data sources are the same as in Fig. 5.

the late-stage evolution of the Paleo-Asian Ocean. During this period, the occurrence of oceanic-ridge subduction would have reduced the subduction angle of the downgoing plate (e.g., Cooke et al., 2005), thereby inducing a compressional tectonic setting and subsequent regional orogenesis and crustal deformation (e.g., Rosenbaum et al., 2005; Li and Li, 2007; Deng et al., 2019; Fig. 17b).

5.3. Mantle contribution and crustal reworking during continental growth in the eastern CAOB

Our study reveals that multi-stage, complex-sourced, and extensive tectonic–magmatic activity occurred in the eastern CAOB during the Permian (Fig. 16). The processes of Early Permian crustal extension and Middle–Late Permian crustal shortening are expected to have resulted in substantial structural modification. It is generally considered that there are two mechanisms of crustal growth: vertical growth by underplating of mantle-derived magmas, and lateral growth by accretion of arc complexes in accretionary orogenic belts (Sengör et al., 1993; Jahn et al., 2000). Mafic intrusive rocks in the eastern CAOB consist mainly of gabbro, diabase, gabbro-diorite, and diorite (Chen et al., 2012; Yu et al., 2013b; Sun et al., 2015; Yang et al., 2015a; Guo et al., 2016; Dong et al., 2017b; Wang et al., 2019, 2020c), most of which were formed by partial melting of metasomatized mantle altered by fluids released from oceanic slab or crustal melts (Fig. 17; Yu et al., 2013b; Bi et al., 2015; Li et al., 2022; Liu et al., 2020). The mafic rocks formed continuously throughout the Permian (Figs. 15d and 16c), indicating sustained subduction of the oceanic slab (Miao et al., 2008; Cao et al., 2013; Li et al., 2015; Pang et al., 2017; Cheng et al., 2020), which led to prolonged continental growth in the eastern CAOB. Scattered Permian adakitic rocks from Xi Ujimqin, Inner Mongolia, are regarded to have been sourced from the subducted oceanic slab (Li et al., 2022), indicating a contribution by oceanic lithosphere to continental crustal growth. The consistent involvement of both mantle and oceanic-crustal materials during the Permian indicates vertical accretion in the eastern CAOB that was driven by the subduction of oceanic lithosphere.

In addition to continental accretion triggered by the addition of mantle and oceanic lithosphere materials, tectonic activity also caused the remobilization of crustal materials (Figs. 16 and 17). The occurrences of Permian adakitic and I-, S-, and A-type granites indicate large-scale remelting of the continental crust (Figs. 15e, f and 16d). Permian granites in the Jiamusi Block and adjacent northern NCC yield negative $\varepsilon_{Hf}(t)$ values (Fig. 8), implying the involvement of ancient crustal materials. In contrast, Permian granites in the Songnen Block yield positive $\varepsilon_{Hf}(t)$ values (Fig. 8), indicating the remelting of juvenile basaltic lower crust with limited involvement of ancient crustal materials. On the basis of the petrogenesis of different igneous rocks and associated regional tectonic evolution, as discussed above, we propose that vertical crustal growth in the eastern CAOB was driven predominantly by large-scale continental crustal reworking.

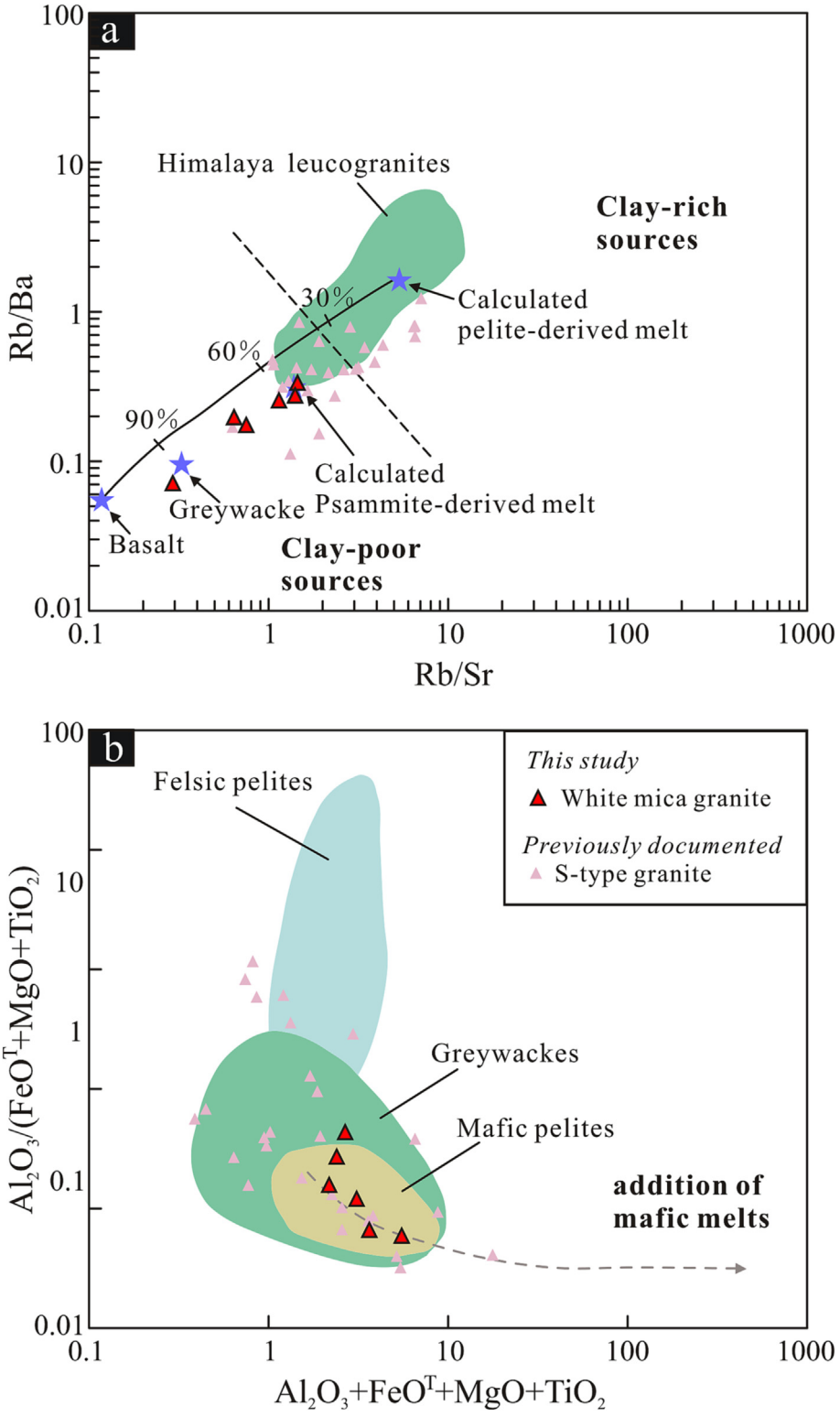

Fig. 13. Plots of (a) Rb/Ba vs. Rb/Sr (after Sylvester, 1998), and (b) $Al_2O_3/(FeO^T + MgO + TiO_2)$ vs. $Al_2O_3 + FeO^T + MgO + TiO_2$ (after Patiño Douce, 2012) for Permian S-type granites from the eastern CAOB. Data sources are the same as in Fig. 5.

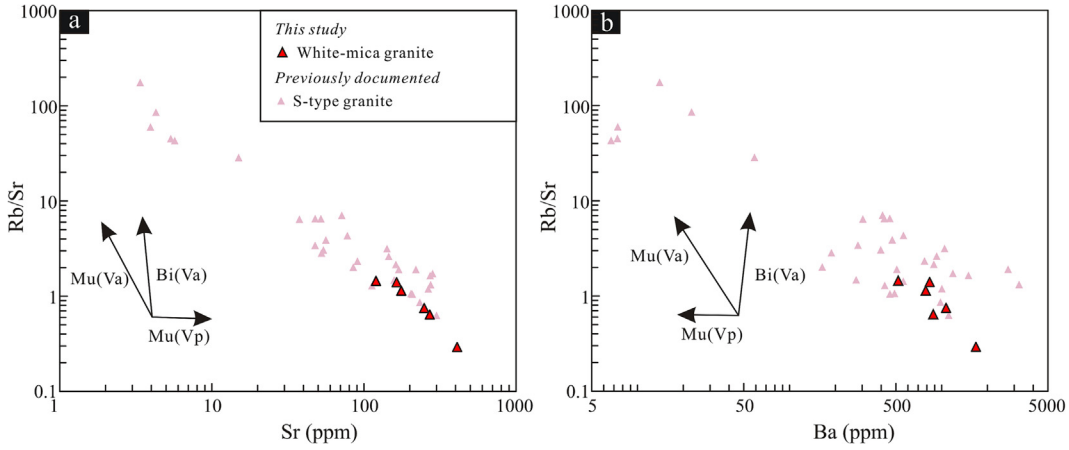

Fig. 14. Plots of (a) Rb/Sr vs. Sr and (b) Rb/Sr vs. Ba (after Inger and Harris, 1993) for Permian S-type granites from the eastern CAOB. Data sources are the same as in Fig. 5.

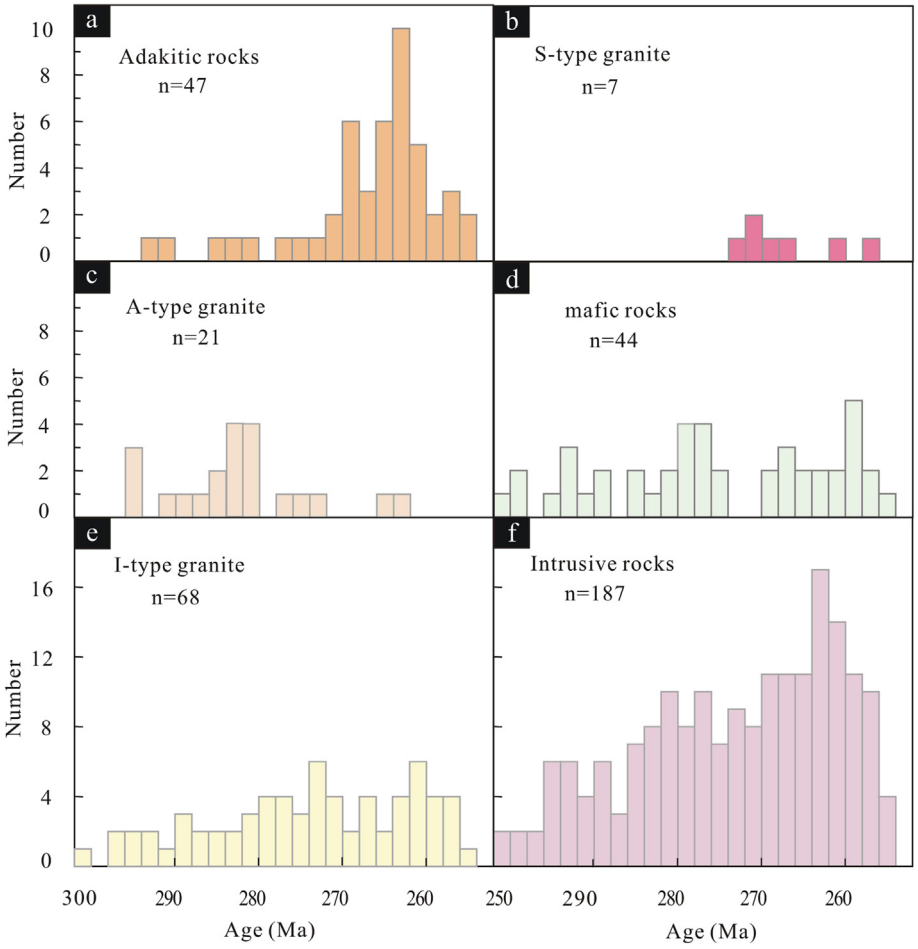

Fig. 15. Frequency plots of isotopic ages of Permian igneous rocks from the eastern CAOB and adjacent areas. (a) All intrusive rocks; (b) I-type granites; (c) adakitic rocks; (d) S-type granites; (e) A-type granites; (f) mafic rocks. Histogram bins are 2 Ma. The compiled geochronological data are listed in Supplementary Data Table S6.

6. Conclusion

The occurrence of different-types of granitoid, including adakitic and S-, I-, and A-type granites, reveals a complex tectonic evolution and extensive reworking of continental materials in the eastern CAOB during the Permian. A-type granites formed predominantly during the Early-Middle Permian, whereas S- and adakitic granites were emplaced mainly during the Middle-Late Permian. This temporal pattern of compositional variation indicates that the eastern CAOB was in an extensional setting during the Early Permian and a compressional setting during the Late Permian; i.e., a transition from an extensional to compressional setting occurred during the Middle Permian. This transition was associated with the gradual narrowing and closure of the Paleo-Asian

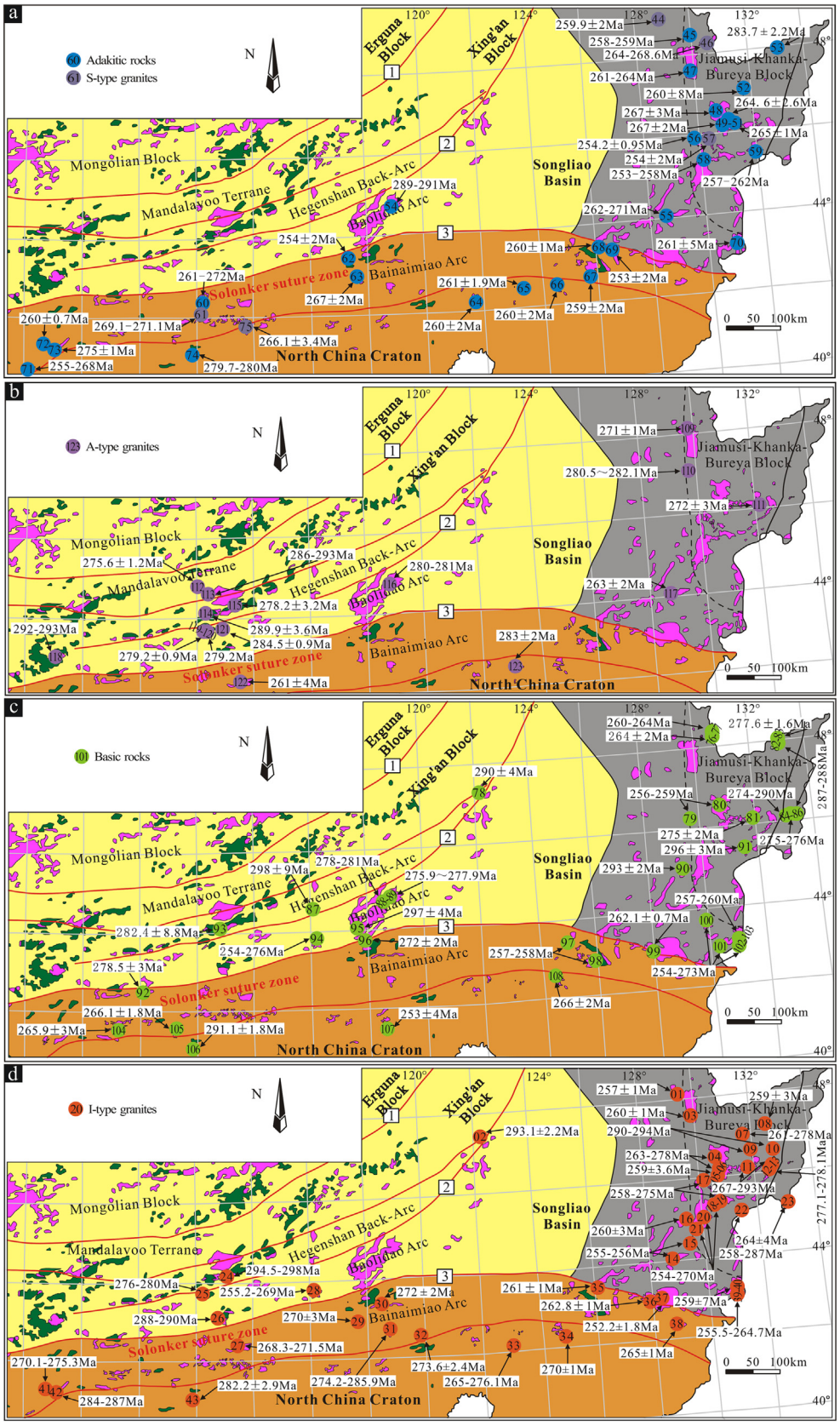

Fig. 16. Geological maps showing the temporal-spatial distribution of Permian igneous rocks in the eastern CAOB and adjacent areas. (a) I-type granites; (b) adakitic and S-type granites; (c) mafic rocks; (d) A-type granites. The compiled geochronological data are listed in Supplementary Data Table S6.

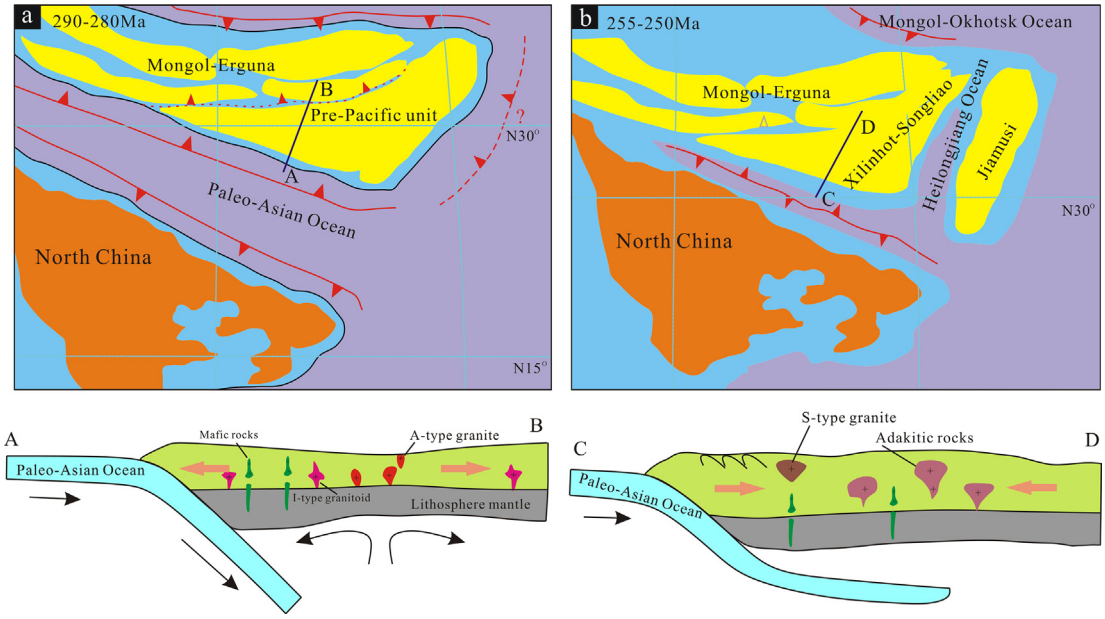

Fig. 17. Diagrams showing the paleogeographic evolution of the eastern CAOB during the Permian (modified after Zhu et al., 2022) and the subduction model proposed in this study for the (a) Early and (b) Late Permian geodynamic evolution of the eastern CAOB.

Ocean, which led to the collision of the CAOB and NCC during the Late Permian–Early Triassic. In addition, extensively distributed Permian mantle-derived mafic rocks in the eastern CAOB indicate substantial mantle contribution to continental crustal growth in the eastern CAOB.

CRediT authorship contribution statement

Anzong Fu: Conceptualization, Data curation, Formal analysis, Investigation, Writing-original draft. **Hongyan Geng**: Conceptualization, Formal analysis, Writing-original draft, Writing-review & editing. **Changzhou Deng**: Conceptualization, Data curation, Formal analysis, Funding acquisition, Project administration, Investigation, Methodology, Writing-original draft, Writing-review & editing. **Jishuang Ding**: Formal analysis, Investigation, Writing-original draft. **Chenglu Li**: Investigation, Writing-original draft, Resources, Supervision. **Bizheng Yang**: Investigation, Data curation, Formal analysis. **Wenpeng Yang**: Investigation, Data curation, Formal analysis.

Declaration of competing interest

The authors declare that they have no known competing financial interests or personal relationships that could have appeared to influence the work reported in this paper.

Acknowledgements

We would like to thank Editorial Advisor M. Santosh, Handling Editor Sanghoon Kwon, Editorial Assistant Mudan Yin and anonymous reviewers for the constructive suggestions of the manuscript. This work was financially supported by the Regional Geological Research Program of Geological Survey of China (12120113057600) and the Croucher Chinese Visitorships from Croucher Foundation (2020–2021).

Appendix A. Supplementary data

Supplementary data to this article can be found online at https://doi.org/10.1016/j.gsf.2023.101775.

References

Atherton, M.P., Petford, N., 1993. Generation of sodium-rich magmas from newly underplated basaltic crust. Nature 362, 144–146.
Bai, C.L., Sun, J.G., Zhao, C.T., Qin, K.Z., Liu, Y., Chu, X.L., Xu, Z.K., Li, Y.X., 2021. The multiple mineralizations and geodynamic settings of the Laozuoshan Cu-Au deposit in the Jiamusi Massif, NE China: Zircon U-Pb geochronological, elemental and Hf isotopic geochemical evidence. Ore Geol. Rev. 137, 104291.
Barbarin, B., 1996. Genesis of the two main types of peraluminous granitoids. Geology 24, 295–298.
Bi, J.H., Ge, W.C., Yang, H., Zhao, G.C., Yu, J.J., Zhang, Y.L., Wang, Z.H., Tian, D.X., 2014. Petrogenesis and tectonic implications of early Paleozoic granitic magmatism in the Jiamusi Massif, NE China: Geochronological, geochemical and Hf isotopic evidence. J. Asian Earth Sci. 96, 308–331.
Bi, J.H., Ge, W.C., Yang, H., Zhao, G.C., Xu, W.L., Wang, Z.H., 2015. Geochronology, geochemistry and zircon Hf isotopes of the Dongfanghong gabbroic complex at the eastern margin of the Jiamusi Massif, NE China: Petrogensis and tectonic implications. Lithos 234–235, 27–46.
Bi, J.H., Ge, W.C., Yang, H., Wang, Z.H., Xu, W.L., Yang, J.H., Xing, D.H., Chen, H.J., 2016. Geochronology and geochemistry of late Carboniferous-middle Permian I- and A-type granites and gabbro–diorites in the eastern Jiamusi Massif, NE China: Implications for petrogenesis and tectonic setting. Lithos 266–267, 213–232.
Broska, I., Williams, C.T., Uher, P., Konecny, P., Leichmann, J., 2004. The geochemistry of phosphorus in different granite suites of the Western Carpathians, Slovakia: the role of apatite and P-bearing feldspar. Chem. Geol. 205 (1), 1–15.
Cao, H.H., Xu, W.L., Pei, F.P., Wang, Z.W., Wang, F., Wang, Z.J., 2013. Zircon U-Pb geochronology and petrogenesis of the Late Paleozoic-Early Mesozoic intrusive rocks in the eastern segment of the northern margin of the North China Block. Lithos 170–171, 191–207.
Castillo, P.R., 2006. An overview of adakite petrogenesis. Chin. Sci. Bull. 51 (3), 258–268.
Castillo, P.R., Janney, P.E., Solidum, R.U., 1999. Petrology and geochemistry of Camiguin Island, southern Philippines: insights to the source of adakites and other lavas in a complex arc setting. Contrib. Mineral. Petrol. 134 (1), 33–51.
Chai, H., Ma, Y.F., Santosh, M., Hao, S.L., Luo, T.W., Fan, D.Q., Gao, B., Zong, L.B., Mao, H., Wang, Q.F., 2020. Late Carboniferous to Early Permian oceanic subduction in central Inner Mongolia and its correlation with the tectonic evolution of the southeastern Central Asian Orogenic Belt. Gondwana Res. 84, 245–259.
Chappell, B.W., 1999. Aluminum saturation in I- and S-type granites and the characterization of fractionated haplogranites. Lithos 46 (3), 535–551.
Chappell, B.W., White, A.J.R., 1974. Two contrasting granite types. Pacific Geology 8, 173–174.
Chen, B., Jahn, B.M., Wilde, S., Xu, B., 2000. Two contrasting Paleozoic magmatic belts in northern Inner Mongolia, China: petrogenesis and tectonic implications. Tectonophysics 328 (1–2), 157–182.
Chen, B., Jahn, B.M., Tian, W., 2009. Evolution of the Solonker suture zone: Constraints from zircon U-Pb ages, Hf isotopic ratios and wholerock Nd-Sr isotope compositions of subduction- and collision-related magmas and forearc sediments. J. Asian Earth Sci. 34, 245–257.

Chen, C., Zhang, Z.C., Guo, Z.J., Li, J.F., Feng, Z.S., Tang, W.H., 2012. Geochronology, geochemistry, and its geological significance of the Permian Mandula mafic rocks in Damaoqi, Inner Mongolia. Sci. China Earth Sci. 55 (01), 39–52.
Chen, Z., Zhou, J.B., Li, G.Y., Wilde, S.A., 2023. The nature and spatial-temporal evolution of suture zones in Northeast China. Earth Sci. Rev. 241, 104437.
Cheng, Y.H., Duan, L.F., Wang, S.Y., Li, Y., Teng, X.J., Zhang, T.F., 2020. Termination of the Hegenshan Orogen in the Xing'an–Mongolian Orogenic Belt, North China: geochemical and zircon U-Pb geochronological constraints from Early Permian mafic dykes. Geol. J. 55 (01), 845–861.
Collins, W.J., Richards, S.W., 2008. Geodynamic significance of S-type granites in circum Pacific orogens. Geology 36, 559–562.
Cong, Z.C., Sun, F.Y., Wang, G., Wang, Y.D., Liang, H., Pan, Z.C., Cao, H.l., 2016. Zircon U-Pb age and geochemistry of the magmatic rocks in the Jiamusi massif, NE China and their tectonic implications. Acta Petrol. Sin. 32 (04), 1141–1152 (in Chinese with English abstract).
Cooke, D.R., Hollings, P., Walsh, J.L., 2005. Giant porphyry deposits: Characteristics, distribution, tectonic controls. Econ. Geol. 100, 801–818.
Cui, P.L., Sun, J.G., Han, S.J., Zhang, P., Zhang, Y., Bai, L.A., Gu, A.L., 2013. Zircon U-Pb-Hf isotopes and bulk rock geochemistry of gneissic granites in the northern Jiamusi Massif, Central Asian orogenic belt: implications for Middle Permian collisional orogeny and Mesoproterozoic crustal evolution. Int. Geol. Rev. 55 (9–10), 1109–1125.
Defant, M.J., Drummond, M.S., 1990. Derivation of some modern arc magmas by melting of young subducted lithosphere. Nature 347, 662–665.
Deng, C.Z., Sun, D.Y., Han, J.S., Chen, H.Y., Li, G.H., Xiao, B., Li, R.C., Feng, Y.Z., Li, C.L., Lu, S., 2019. Late-stage southwards subduction of the Mongol-Okhotsk oceanic slab and implications for porphyry Cu-Mo mineralization: Constraints from igneous rocks associated with the Fukeshan deposit, NE China. Lithos 326–327, 341–357.
Deng, C.Z., Lehmann, B., Xiao, T.T., Tan, Q.P., Chen, D., Tian, Z.D., Wang, X.Y., Sun, G. Y., Yin, R.S., 2022. Intracontinental and arc-related hydrothermal systems display distinct δ^{202}Hg and Δ^{199}Hg features: Implication for large-scale mercury recycling and isotopic fractionation in different tectonic settings. Earth Planet. Sci. Lett. 593, 117646.
Ding, J.S., Deng, C.Z., Feng, Y.Z., Yang, Y.B., Zhao, R.J., 2022. Contrasting tectonic regimes between late Jurassic and Early Cretaceous porphyry-epithermal Cu-Mo-Au mineralization in NE China: A perspective from the petrogenesis of the adakitic rocks in the Sishanlinchang porphyry Cu-Mo deposit. Ore Geol. Rev. 148, 105035.
Dokuz, Dokuz, A., Tanyolu, E., Genc, S., 2006. A mantle- and a lower crust-derived bimodal suite in the Yusufeli (Artvin) area, NE Turkey: trace element and REE evidence for subduction-related rift origin of Early Jurassic Demirkent intrusive complex. Int. J. Earth Sci. 95, 370–394.
Dong, Y., Ge, W.C., Yang, H., Bi, J.H., Wang, Z.H., Xu, W.L., 2017a. Permian tectonic evolution of the Mudanjiang Ocean: Evidence from zircon U-Pb-Hf isotopes and geochemistry of a N-S trending granitoid belt in the Jiamusi Massif, NE China. Gondwana Res. 47, 147–163.
Dong, Y., Ge, W.C., Yang, H., Xu, W.L., Bi, J.H., Wang, Z.H., 2017b. Geochemistry and geochronology of the Late Permian mafic intrusions along the boundary area of Jiamusi and Songnen-Zhangguangcai Range massifs and adjacent regions, northeastern China: Petrogenesis and implications for the tectonic evolution of the Mudanjiang Ocean. Tectonophysics 694, 356–367.
Dong, Y., Ge, W.C., Yang, H., Liu, X.W., Bi, J.H., Ji, Z., Xu, W.L., 2019. Geochemical and SIMS U-Pb rutile and LA-ICP-MS U-Pb zircon geochronological evidence of the tectonic evolution of the Mudanjiang Ocean from amphibolites of the Heilongjiang Complex, NE China. Gondwana Res. 69, 25–44.
Drummond, M.S., Defant, M.J., Kepezhinskas, P.K., 1996. Petrogenesis of slab-derived trondhjemite–tonalite–dacite/adakite magmas. Earth Environ. Sci. Trans. R. Soc. Edinb. 87, 205–215.
Eby, G.N., 1992. Chemical subdivision of the A-type granitoids: petrogenetic and tectonic implications. Geology 20, 641–644.
Eizenhöfer, P.R., Zhao, G.C., 2018. Solonker Suture in East Asia and its bearing on the final closure of the eastern segment of the Palaeo-Asian Ocean. Earth Sci. Rev. 186, 153–172.
Eizenhöfer, P.R., Zhao, G.C., Sun, M., Zhang, J., Han, Y.G., Hou, W.Z., 2015. Geochronological and Hf isotopic variability of detrital zircons in Paleozoic strata across the accretionary collision zone between the North China craton and Mongolian arcs and tectonic implications. Geol. Soc. Am. Bull. 127, 1422–1436.
Fu, A.Z., Yang, W.P., Liu, Y., Zhao, H.D., Wang, G.P., Shi, G.M., Li, J.M., Deng, C.Z., 2022. Discovery of Late Triassic adakitic rocks at Nianzishan in the Central Great Xing'an Range and its geological significance. Geoscience 36 (01), 266–281 (in Chinese with English abstract).
Gao, Y., Hao, Y.J., Ren, Y.S., Shi, Y.F., Sun, Z.M., Wang, C.Y., 2020. U-Pb dating of detrital zircon from Dapandao Formation of Xingdong Group in Jiamusi Massif, Helongjiang and its geological significance. Global Geology 39 (1), 16–29 (in Chinese with English abstract).
Gao, S., Liu, X.M., Yuan, H.L., Hattendorf, B., Gunther, D., Chen, L., Hu, S.H., 2002. Determination of forty-two major and trace elements in USGS and NIST SRM glasses by laser ablation-inductively coupled plasma-mass spectrometry. Geostand. Geoanal. Res. 26, 181–196.
Guo, F., Nakamuru, E., Fan, W.M., Kobayoshi, K., Li, C.W., 2007. Generation of Palaeocene adakitic andesites by magma mixing; Yanji Area, NE China. J. Petrol. 48 (4), 661–692.
Guo, F., Li, H.X., Fan, W.M., Li, J.Y., Zhao, L., Huang, M.W., 2016. Variable sediment flux in generation of Permian subduction-related mafic intrusions from the Yanbian region, NE China. Lithos 261, 195–215.
Harris, N., Ayres, M., Massey, J., 1995. Geochemistry of granitic melts produced during the incongruent melting of muscovite: implications for the extraction of Himalayan leucogranite magmas. J. Geophys. Res. Solid Earth 100, 15767–15777.
Hu, C.S., Li, W.B., Xu, C., Zhong, R.C., Zhu, F., Qiao, X.Y., 2015a. Geochemistry and petrogenesis of Permian granitoids in the northwestern margin of the North China Craton: insights from the Dongshengmiao pluton, Inner Mongolia. Int. Geol. Rev. 57 (14), 1843–1860.
Hu, P.Y., Zhai, Q.G., Jahn, B.M., 2015b. Early Ordovician granites from the South Qiangtang terrane, northern Tibet: Implications for the early Paleozoic tectonic evolution along the Gondwanan proto-Tethyan margin. Lithos 220–223, 318–338.
Hui, J., Zhang, K.J., Zhang, J., Qu, J.F., Zhang, B.H., Zhao, H., Niu, P.F., 2021. Middle–late Permian high-K adakitic granitoids in the NE Alxa block, northern China: Orogenic record following the closure of a Paleo-Asian oceanic branch? Lithos 400–401, 106379.
Inger, S., Harris, N., 1993. Geochemical constraints on leucogranite magmatism in the Langtang Valley, Nepal Himalaya. J. Petrol. 34 (2), 345–368.
Irvine, T.N., Baragar, W.R., 1971. A guide to the chemical classification of the common volcanic rocks. Can. J. Earth Sci. 8, 523–548.
Jahn, B.M., 2004. The Central Asian Orogenic Belt and growth of the continental crust in the Phanerozoic. Geol. Soc. London Spec. Publ. 226, 73–100.
Jahn, B.M., Wu, F.Y., Chen, B., 2000. Granitoids of the Central Asian Orogenic Belt and continental growth in the Phanerozoic. Earth Envion. Sci. Trans. R. Soc. Edinb 91 (1–2), 181–193.
Ji, Z.J., Zhang, Z.C., Yang, J.F., Chen, Y., Tang, J.Z., 2020. Carboniferous-Early Permian sedimentary rocks from the north-eastern Erenhot, North China: Implications on the tectono-sedimentary evolution of the south-eastern Central Asian Orogenic Belt. Geol. J. 55 (3), 2383–2401.
Jiang, Y.H., Jia, R.Y., Liu, Z., Liao, S.Y., Zhao, P., Zhou, Q., 2013. Origin of Middle Triassic high K calc-alkaline granitoids and their potassic microgranular enclaves from the western Kunlun orogeny, northwest China: a record of the closure of Paleo-Tethys. Lithos 156–159, 13–30.
Jing, Y., Ge, W.C., Santosh, M., Dong, Y., Yang, H., Zheng, J., Bi, J.H., Zhou, H.Y., Xing, D. H., 2022. Generation of Nb-enriched mafic rocks and associated adakitic rocks from the southeastern Central Asian Orogenic Belt: Evidence of crust-mantle interaction. Geosci. Front. 13, 101341.
Kang, Z.Q., Xu, J.F., Chen, J.L., Wang, B.D., 2009. Geochemistry and origin of Cretaceous adakites in Mamuxia Formation, Sangri Group, South Tibet. Geochimica 38 (4), 334–344 (in Chinese with English abstract).
Kelty, T.K., Yin, A., Dash, B., Gehrels, G.E., Ribeiro, A.E., 2008. Detrital-zircon geochronology of Paleozoic sedimentary rocks in the Hangay-Hentey basin, north-central Mongolia: implications for the tectonic evolution of the Mongol-Okhotsk Ocean in central Asia. Tectonophysics 451, 290–311.
Kepezhinskas, P., McDermott, F., Defant, M.J., Hochstaedter, A., Drummond, M.S., Hawkesworth, C.J., Koloskov, A., Maury, R.C., Bellon, H., 1997. Trace element and Sr-Nd-Pb isotopic constraints on a three-component model of Kamchatka arc petrogenesis. Geochim. Cosmochim. Acta 61, 577–600.
Kessel, R., Schmidt, M.W., Ulmer, P., Pettke, T., 2005. Trace element signature of subduction-zone fluids, melts and supercritical liquids at 120–180 km depth. Nature 437, 724–727.
Konopelko, D., Wilde, S.A., Seltmann, R., Romer, R.L., Biske, Y.S., 2018. Early Permian intrusions of the Alai range: Understanding tectonic settings of Hercynian post-collisional magmatism in the South Tien Shan, Kyrgyzstan. Lithos 302 (1), 405–420.
Konopelko, D., Biske, Y.S., Kullerud, K., Ganiev, I., Seltmann, R., Brownscombe, W., Mirkamalov, R., Wang, B., Safonova, I., Kotler, P., 2019. Early Carboniferous metamorphism of the Neoproterozoic South Tien Shan-Karakum basement: New geochronological results from Baisun and Kyzylkum, Uzbekistan. J. Asian Earth Sci. 177, 275–286.
Konopelko, D., Seltmann, R., Dolgopolova, A., Safonova, I., Glorie, S., Grave, J.D., Sun, M., 2021. Adakite-like granitoids of Songkultau: A relic of juvenile Cambrian arc in Kyrgyz Tien Shan. Geosci. Front. 12 (1), 147–160.
Koschek, G., 1993. Origin and significance of the SEM cathodoluminescence from zircon. J. Microsc. Oxford. 171 (3), 223–232.
Labanieh, S., Chauvel, C., Germa, A., Quidelleur, X., 2012. Martinique: a clear case for sediment melting and slab dehydration as a function of distance to the trench. J. Petrol. 53, 2441–2464.
Li, J.Y., Guo, F., Li, C.W., Zhao, L., Huang, M.W., 2015. Permian back-arc extension in central Inner Mongolia, NE China: Elemental and Sr-Nd-Pb-Hf-O isotopic constraints from the Linxi high-MgO diabase dikes. Isl. Arc 24 (04), 404–424.
Li, X.P., Kong, F.M., Zheng, Q.D., Dong, X.A., Yang, Z.Y., 2010. Geochronological study on the Heilongjiang complex at Luobei area, Heilongjiang Province. Acta Petrol. Sin. 26 (7), 2015–2024 (in Chinese with English abstract).
Li, X.H., Li, Z.X., Zhou, H.W., Liu, Y., Kinny, P.D., 2002. U-Pb zircon geochronology, geochemistry and Nd isotopic study of Neoproterozoic bimodal volcanic rocks in the Kangdian Rift of South China: implications for the initial rifting of Rodinia. Precambrian Res. 113, 135–154.
Li, Z.X., Li, X.H., 2007. Formation of the 1300-km-wide intracontinental orogen and postorogenic magmatic province in Mesozoic South China: A flat-slab subduction model. Geology 35 (2), 179–182.

Li, W.M., Liu, Y.J., Zhao, Y.L., Feng, Z.Q., Zhou, J.P., Wen, Q.B., Liang, C.Y., Zhang, D., 2020b. Tectonic evolution of the Jiamusi Block, NE China. Acta Petrol. Sin. 36 (3), 665–684 (in Chinese with English abstract).
Li, J.L., Liu, J.G., Scott, J.M., Wu, C., Zhu, D.C., Zhang, L.L., 2022. Early Permian magmatism above a slab window in Inner Mongolia, North China: Implications for the Paleo-Asian Ocean subduction processes and accretionary crustal growth. Solid Earth Sci. 7 (2), 87–103.
Li, W.M., Takasu, A., Liu, Y.J., Genser, J., Zhao, Y.L., Han, G.Q., Guo, X.Z., 2011. U-Pb and $^{40}Ar/^{39}Ar$ age constrains on protolith and high-P/T type metamorphism of the Heilongjiang Complex in the Jiamusi Massif, NE China. J. Miner. Petrol. Sci. 106 (6), 326–331.
Li, Y.L., Wang, G.Q., Xiao, W.J., Zuo, J., Zheng, J.P., Fraukje, M.B., 2019. Detrital zircon U-Pb ages and geochemistry of the Silurian to Permian sedimentary rocks in Central Inner Mongolia, China: Implications for closure of the Paleo-Asian Ocean. Acta Geol. Sin.-Engl. 93, 1228–1260.
Li, J., Wang, K.Y., Fu, L.J., Zhang, M., Liu, Q.Z., Tang, W.H., Wang, C.H., 2020a. Adakitic rocks and A-type felsic dykes in the Changlingzi area, NE China: Constraints on multistage tectonism in the southern Great Xing'an Range. Geol. J. 55 (7), 5451–5478.
Li, Y., Xu, W.L., Wang, F., Tang, J., Zhao, S., Guo, P., 2017. Geochronology and geochemistry of late Paleozoic–early Mesozoic igneous rocks of the Erguna Massif, NE China: Implications for the early evolution of the Mongol-Okhotsk tectonic regime. J. Asian Earth Sci. 144, 205–224.
Li, H.H., Yu, J.J., Guo, X.W., Xu, W.L., 2021. Late Permian medium-pressure metamorphism in the eastern Songnen Massif, eastern Central Asian Orogenic Belt (NE China): Implications for the final closure of the Paleo-Asian Ocean. J. Asian Earth Sci. 215, 104800.
Liao, Z.L., Mo, X.X., Pan, G.T., Zhu, D.C., Wang, L.Q., Zhao, Z.D., Geng, Q.R., Dong, G.C., 2006. Quzhen peraluminous granite, Tibet: Geochemical characteristics and geodynamic significance. Acta Petrol. Sin. 22 (4), 845–854 (in Chinese with English abstract).
Liu, Y.S., Gao, S., Hu, Z.C., Gao, C.G., Zong, K.Q., Wang, D.B., 2010. Continental and oceanic crust recycling-induced melt-peridotite interactions in the Trans-North China Orogen: U-Pb dating, Hf isotopes and trace elements in zircons of mantle xenoliths. J. Petrol. 51, 537–571.
Liu, J., Zhang, J., Liu, Z.H., Yin, C.Q., Zhao, C., Yu, X.Y., Chen, Y., Tian, Y., Dong, Y., 2020. Petrogenesis of Permo-Triassic intrusive rocks in Northern Liaoning Province, NE China: implications for the closure of the eastern Paleo-Asian Ocean. Int. Geol. Rev. 62 (6), 754–780.
Luan, J.P., Tang, J., Xu, W.L., Tian, Y., Guo, P., Wang, J.G., Li, Y., 2022. Accretion kinematics and driving mechanism of the eastern Central Asian Orogenic Belt: Insights from seismic tomography and middle Permian-Middle Triassic magmatism in central Jilin Province. Gondwana Res. 101, 114–131.
Ludwig, K.R., 2003. ISOPLOT 3.00: A Geochronological Toolkit for Microsoft Excel. Berkeley Geochronology Center, California, Berkeley, p. 39.
Ma, H.W., 1992. Discrimination of genetic types of granitoid rocks. Acta Petrol. Sin. 08 (04), 341–350 (in Chinese with English abstract).
Ma, Y.F., Liu, Y.J., Wang, Y., Qian, C., Si, Q.L., Tang, Z., Qin, T., 2019. Geochronology, petrogenesis, and tectonic implications of Permian felsic rocks of the Central Great Xing'an Range, NE China. Int. J. Earth Sci. 108, 427–453.
Maniar, P.D., Piccoli, P.M., 1989. Tectonic discrimination of granitoids. Geol. Soc. Am. Bull. 101, 635–643.
McDonough, W.F., Sun, S.S., 1995. The composition of the Earth. Chem. Geol. 120 (3–4), 223–253.
McKenzie, D., O'Nions, R.K., 1991. Partial melt distribution from inversion of rare earth element concentrations. J. Petrol. 32, 1021–1091.
Metelkin, D.V., Vernikovsky, V.A., Kazansky, A.Y., Wingate, M.T.D., 2010. Late Mesozoic tectonics of Central Asia based on paleomagnetic evidence. Gondwana Res. 18, 400–419.
Miao, L.C., Fan, W.M., Liu, D.Y., Zhang, F.Q., Shi, Y.R., Guo, F., 2008. Geochronology and geochemistry of the Hegenshan ophiolitic complex: Implications for late-stage tectonic evolution of the Inner Mongolia-Daxinganling Orogenic Belt, China. J. Asian Earth Sci. 32 (5–6), 348–370.
Miller, C.F., Mcdowell, S.M., Mapes, R.W., 2003. Hot and cold granites? Implications of zircon saturation temperatures and preservation of inheritance. Geology 31 (6), 529–532.
Nokleberg, W.J., Parfenov, L.M., Monger, J.W.H., Norton, I.O., Khanchuk, A.I., Stone, D. B., Scotese, C.R., Scholl, D.W., Fujita, K., 2000. Phanerozoic Tectonic Evolution of the Circum-North Pacific. U.S. Geological Survey Professional Paper 1626, pp. 122.
Pang, C.J., Wang, X.C., Xu, B., Luo, Z.W., Liu, Y.Z., 2017. Hydrous parental magmas of Early to Middle Permian gabbroic intrusions in western Inner Mongolia, North China: New constraints on deep-Earth fluid cycling in the Central Asian Orogenic Belt. J. Asian Earth Sci. 144, 184–204.
Patiño Douce, A.E., 2005. Vapor-absent melting of tonalite at 15–32 kbar. J. Petrol. 46, 275–290.
Patiño Douce, A.E., 2012. What do experiments tell us about the relative contributions of crust and mantle to the origin of granitic magmas? Geol. Soc. London Spec. Publ. 168, 55–75.
Pearce, J.A., 1982. Trace element characteristics of lavas from destructive plate boundaries. In: Thorpe, R.S. (Ed.), Andesites: Orogenic Andesites and Related Rocks. John Wiley and Sons, New York, pp. 525–548.
Pearce, J.A., 1983. The role of sub-continental lithosphere in magma genesis at destructive plate margins. In: Hawkesworth, C.J., Norry, M.J. (Eds.), Continental Basalts and Mantle Xenoliths. Shiva, Nantwich, pp. 230–249.
Peccerillo, A., Taylor, S.R., 1976. Geochemistry of Eocene calc-alkaline volcanic rocks from the Kastamonu area, northern Turkey. Contrib. Mineral. Petrol. 58, 63–81.
Ren, L.D., Wang, Y.B., Yang, C.H., Zhao, Z.R., Guo, J.J., Gao, H.L., 2012. Two types of metamorphism and their relationships with granites in the Mashan Complex. Acta Petrol. Sin. 28 (9), 2855–2865 (in Chinese with English abstract).
Rosenbaum, G., Giles, D., Saxon, M., Bette, P.G., Weinberg, R.F., Duboz, C., 2005. Subduction of the Nazca Ridge and the Inca Plateau: Insights into the formation of ore deposits in Peru. Earth Planet. Sci. Lett. 239, 18–32.
Safonova, I.Y., Santosh, M., 2014. Accretionary complexes in the Asia-Pacific region: tracing archives of ocean plate stratigraphy and tracking mantle plumes. Gondwana Res. 25, 126–158.
Sajona, F.G., Maury, R.C., Bellon, H., Cotten, J., Defant, M., 1996. High field strength element enrichment of Pliocene-Pleistocene Island arc basalts, Zamboanga peninsula, Western Mindanao (Philippines). J. Petrol. 37 (3), 693–726.
Sajona, F.G., Maury, R.C., Pubellier, M., Leterrier, J., Bellon, H., Cotten, J., 2000. Magmatic source enrichment by slab-derived melts in a young post-collision setting, central Mindanao (Philippines). Lithos 54 (3–4), 173–206.
Sengör, A.M.C., Natal'in, B.A., Burtman, V.S., 1993. Evolution of the Altaid tectonic collage and Paleozoic crustal growth in Eurasia. Nature 364, 299–307.
Shen, Y., Zheng, Y.C., Hou, Z.Q., Zhang, A.P., Huizenga, J.M., Wang, Z.X., Wang, L., 2021. Petrology of the Machangqing complex in southeastern Tibet: Implications for the genesis of potassium-rich Adakite-like intrusions in collisional zones. J. Petrol. 62, 1–40.
Shi, Y., Liu, Z.H., Liu, Y.J., Shi, S.S., Wei, M.H., Yang, J.J., Gao, T., 2019. Late Paleozoic-Early Mesozoic southward subduction-closure of the Paleo-Asian Ocean: Proof from geochemistry and geochronology of Early Permian-Late Triassic felsic intrusive rocks from North Liaoning, NE China. Lithos 346–347, 105165.
Sláma, J., Kosler, J., Condon, D.J., Crowley, J.L., Gerdes, A., Hanchar, J.M., Horstwood, M.S.A., Morris, G.A., Nasdala, L., Norberg, N., Schaltegger, U., Schoene, B., Tubrett, M.N., Whitehouse, M.J., 2008. Plesovice zircon-A new natural reference material for U-Pb and Hf isotopic microanalysis. Chem. Geol. 249, 1–35.
Song, D.F., Xiao, W.J., Collins, A.S., Glorie, S., Han, C.M., Li, Y.C., 2018. Final subduction processes of the Paleo-Asian Ocean in the Alxa Tectonic Belt (NW China): Constraints from field and chronological data of Permian arc-related volcano sedimentary rocks. Tectonics 37, 1658–1687.
Sorokin, A.A., Kudryashov, N.M., Kotov, A.B., Kovach, V.P., 2017. Age and tectonic setting of the early Paleozoic magmatism of the Mamyn Terrane, Central Asian Orogenic Belt, Russia. J. Asian Earth Sci. 144, 22–39.
Stern, R.J., 2002. Subduction zones. Rev. Geophys. 40 (4), 1012.
Streck, M.J., Leeman, W.P., Chesley, J., 2007. High-magnesian andesite from Mount Shasta: A product of magma mixing and contamination, not a primitive mantle melt. Geology 35 (1), 351–354.
Sun, S.S., McDonough, W., 1989. Chemical and isotopic systematics of oceanic basalts: implications for mantle composition and processes. Geol. Soc. London Spec. Publ. 42, 313–345.
Sun, M.D., Xu, Y.G., Wilde, S.A., Chen, H.L., Yang, S.F., 2015. The Permian Dongfanghong island-arc gabbro of the Wandashan Orogen, NE China: Implications for Paleo-Pacific subduction. Tectonophysics 659, 122–136.
Sylvester, P.J., 1998. Post-collisional strongly peraluminous granites. Lithos 45, 29–44.
Tang, J., Li, A.P., Xu, W.L., 2020. Geochronology and geochemistry of late Carboniferous-Middle Jurassic magmatism in the Helong area, NE China: Implications for the tectonic transition from the Paleo-Asian oceanic to circum-Pacific regime. Geol. J. 55, 1808–1825.
Taylor, S.R., McLennan, S.M., 1985. The continental crust: Its composition and evolution, an examination of the geochemical record preserved in sedimentary rocks. Blackwell Scientific Pub, Oxford, p. 312.
Tong, Y., Jahn, B.M., Wang, T., Hong, D.W., Smith, E.I., Sun, M., Gao, J.F., Yang, Q.D., Huang, W., 2015. Permian alkaline granites in the Erenhot-Hegenshan belt, northern Inner Mongolia, China: Model of generation, time of emplacement and regional tectonic significance. J. Asian Earth Sci. 97, 320–336.
Wang, Y., Gao, Y.F., Santosh, M., Hou, Z.Q., Zhang, H.R., Xu, S.C., 2020c. Permian dyke swarm with bimodal affinity from the Hegenshan ophiolite-arc-accretionary belt, Central Inner Mongolia: Implications on lithospheric extension in a Carboniferous continental arc. Lithos 356–357, 105369.
Wang, K., Li, Y.L., Xiao, W.J., Zheng, J.P., Fraukje, M.B., 2019. Zircon U-Pb Ages and Geochemistry of Permo-Carboniferous Mafic Intrusions in the Xilinhot Area, Inner Mongolia: Constraints on the Northward Subduction of the Paleo-Asian Ocean. Acta Geol. Sin. Engl. 93 (05), 1261–1280.
Wang, J.X., Nie, F.J., Zhang, X.N., Jiang, S.H., 2016. Molybdenite Re–Os, zircon U-Pb dating and Lu–Hf isotopic analysis of the Xiaerchulu Au deposit, Inner Mongolia Province, China. Lithos 261, 356–372.
Wang, W.L., Teng, X.J., Liu, Y., Wang, R., Cheng, Y.H., Xin, H.T., Wang, S.Q., 2020b. From subduction to post-collision: Early Permian-middle Triassic magmatic records from Langshan Belt, Central Asian Orogenic Belt. Geol. J. 55 (3), 2167–2184.
Wang, Z.J., Xu, W.L., Pei, F.P., Wang, Z.W., Li, Y., Cao, H.H., 2015. Geochronology and geochemistry of middle Permian-Middle Triassic intrusive rocks from central-eastern Jilin Province, NE China: Constraints on the tectonic evolution of the eastern segment of the Paleo-Asian Ocean. Lithos 238, 13–25.
Wang, Q., Zhao, Z.H., Xu, J.F., Bai, Z.H., Wang, J.X., Liu, C.X., 2004. The geochemical comparison between the Tongshankou and Yinzu adakitic intrusive rocks in southeastern Hubei: (delaminated) lower crustal melting and the genesis of porphyry copper deposit. Acta Petrol. Sin. 20 (2), 351–360 (in Chinese with English abstract).

Wang, B.R., Zhou, Z.G., Yang, X.S., Li, S.C., Zhou, Y., Zhang, X.F., Zhang, H.C., 2020a. A Late Carboniferous-Early Permian back-arc basin in the southeastern Central Asian Orogenic Belt: Constraint from sedimentological and geochronological investigations of the Shoushangou Formation in the central Inner Mongolia. Geol. J. 55 (2), 1098–1114.
Weinberg, R.F., Hasalová, P., 2015. Water-fluxed melting of the continental crust: A review. Lithos 212, 158–188.
Wen, Q.B., Liu, Y.J., Gao, F., Li, W.M., Feng, Z.Q., Zhou, J.P., Liang, C.Y., 2017. Thermochronological evidence for multi-phase uplifting and exhumation history the Jiamusi uplift in eastern Heilongjiang, China. Acta Petrol. Sin. 33 (6), 1789–1804 (in Chinese with English abstract).
Whalen, J.B., Currie, K.L., Chappell, B.W., 1987. A-type granites: geochemical characteristics, discrimination and petrogenesis. Contrib. Mineral. Petrol. 95, 407–419.
Wilde, S.A., 2015. Final amalgamation of the Central Asian Orogenic Belt in NE China: Paleo-Asian Ocean closure versus Paleo-Pacifific plate subduction - A review of the evidence. Tectonophysics 662, 345–362.
Wilde, S.A., Dorsett-Bain, H.L., Liu, J.L., 1997. In: The Identification of a Late Pan-African Granulite Facies Event in Northeastern China: SHRIMP U-Pb Zircon Dating of the Mashan Group at Liu. VSP International Science Publishers, Amsterdam, pp. 59–74.
Wilde, S.A., Zhou, J.B., Wu, F.Y., 2015. Development of the north-eastern segment of the Central Asian Orogenic Belt. In: Kroner, A. (Ed.), The Central Asian Orogenic Belt. Contributions to the Regional Geology of the Earth. E. Schweitzerbart Science Publishers, Stuttgart, Germany, pp. 184–210.
Wilde, S.A., Zhang, X.Z., Wu, F.Y., 2000. Extension of a newly identified 500 Ma metamorphic terrane in North East China: further U-Pb SHRIMP dating of the Mashan Complex, Heilongjiang Province, China. Tectonophysics 328, 115–130.
Wilde, S.A., Wu, F.Y., Zhao, G.C., 2010. The Khanka Block, NE China, and its significance for the evolution of the Central Asian Orogenic Belt and continental accretion. Geol. Soc. London Spec. Publ. 338, 117–137.
Windley, B.F., Alexeiev, D., Xiao, W.J., Kroner, A., Badarch, G., 2007. Tectonic models for accretion of the Central Asian Orogenic Belt. J. Geol. Soc. London 164, 31–47.
Wu, F.Y., Sun, D.Y., Li, H.M., Jahn, B., Wilde, S., 2002. A-type granites in northeastern China: age and geochemical constraints on their petrogenesis. Chem. Geol. 187, 143–173.
Wu, F.Y., Yang, Y.H., Xie, L.W., Yang, J.H., Xu, P., 2006. Hf isotopic compositions of the standard zircons and baddeleyites used in U-Pb geochronology. Chem. Geol. 234, 105–126.
Wu, F.Y., Yang, J.H., Lo, C.H., Wilde, S.A., Sun, D.Y., Jahn, B.M., 2007. The Heilongjiang Group: A Jurassic accretionary complex in the Jiamusi Massif at the western Pacific margin of northeastern China. Isl. Arc 16, 156–172.
Wu, F.Y., Sun, D.Y., Ge, W.C., Zhang, Y.B., Grant, M.L., Wilde, S.A., Jahn, B.M., 2011. Geochronology of the Phanerozoic granitoids in northeastern China. J. Asian Earth Sci. 41, 1–30.
Wutiepu, W., Yang, Y.C., Tan, Y., Han, S.J., Guo, Y.F., Wang, Q.S., Wang, X.Y., Wang, F. B., 2018. Geochemistry, geochronology, and geological implications of the granitoids associated with the Dongfengshan gold deposit, Heilongjiang Province, NE China. Geol. J. 53 (05), 2143–2160.
Xiao, W.J., Windley, B.F., Hao, J., Zhai, M.G., 2003. Accretion leading to collision and the Permian Solonker suture, Inner Mongolia, China: termination of the Central Asian Orogenic Belt. Tectonics 22, 1069–1089.
Xiao, W., Windley, B.F., Sun, S., Li, J., Huang, B., Han, C., Yuan, C., Sun, M., Chen, H., 2015. A tale of amalgamation of three permo-triassic collage systems in central Asia: Oroclines, sutures, and terminal accretion. Annu. Rev. Earth Planet. Sci. 43 (1), 477–507.
Xu, G.Z., Deng, C.Z., Li, C.L., Lv, C.L., Yin, R.S., Ding, J.S., Yuan, M.W., Gou, J., 2020. Petrogenesis of Late Carboniferous A-type granites and Early Cretaceous adakites of the Songnen Block, NE China: Implications for the geodynamic evolution of the Paleo-Asian and Paleo-Pacific oceans. Lithos 366–367, 105575.
Xu, W.L., Pei, F.P., Wang, F., Meng, E., Ji, W.Q., Yang, D.B., Wang, W., 2013. Spatial-temporal relationships of Mesozoic volcanic rocks in NE China: constraints on tectonic overprinting and transformations between multiple tectonic regimes. J. Asian Earth Sci. 74, 167–193.
Xu, J.F., Shinjo, R., Defant, M.J., Wang, Q., Rapp, R.P., 2002. Origin of Mesozoic adakitic intrusive rocks in the Ningzhen area of east China: Partial melting of delaminated lower continental crust? Geology 30 (12), 1111–1114.
Xu, W.L., Wang, Y.N., Wang, F., Tang, J., Long, X.Y., Dong, Y., Li, Y., Zhang, X.Z., 2022. Evolution of western Pacific subduction zones: Constraints from accretionary complexes in NE Asian continental margin. Geol. Rev. 68 (1), 1–17 (in Chinese with English abstract).
Yang, H., Ge, W.C., Zhao, G.C., Yu, J.J., Zhang, Y.L., 2015a. Early Permian-Late Triassic granitic magmatism in the Jiamusi-Khanka Massif, eastern segment of the Central Asian Orogenic Belt and its implications. Gondwana Res. 27, 1509–1533.
Yang, H., Ge, W.C., Dong, Y., Bi, J.H., Wang, Z.H., Ji, Z., 2017a. Record of Permian-Early Triassic continental arc magmatism in the western margin of the Jiamusi Block, NE China: petrogenesis and implications for Paleo-Pacific subduction. Int. J. Earth Sci. 106 (6), 1919–1942.
Yang, H., Ge, W.C., Zhao, G.C., Bi, J.H., Wang, Z.H., Dong, Y., Xu, W.L., 2017b. Zircon U-Pb ages and geochemistry of newly discovered Neoproterozoic orthogneisses in the Mishan region, NE China: Constraints on the high-grade metamorphism and tectonic affinity of the Jiamusi-Khanka Block. Lithos 268–271, 16–31.
Yang, Y.T., Guo, Z.X., Song, C.C., Li, X.B., He, S., 2015b. A short-lived but significant Mongol-Okhotsk collisional orogeny in latest Jurassic-earliest Cretaceous. Gondwana Res. 28, 1096–1116.
Yang, J.H., Wu, F.Y., Shao, J.A., Wilde, S.A., Xie, L.W., Liu, X.M., 2006. Constrains on the timing of uplift of the Yanshan Fold and Thrust Belt, North China. Earth Planet. Sci. Lett. 246, 336–352.
Yang, Z.L., Zhang, X.H., Yuan, L.L., 2021. Tracking decratonization process along a cratonic edge through late Permian to late Triassic magmatic flare-up in northwestern Liaoning, North China Craton. Lithos 380–381, 105916.
Yin, R.S., Deng, C.Z., Lehmann, B., Sun, G.Y., Lepak, R.F., Hurley, J.P., Zhao, C.H., Xu, G. W., Tan, Q.P., Xie, Z.J., et al., 2019. Magmatic-hydrothermal origin of Mercury in Carlin-style and epithermal gold deposits in China: Evidence from mercury stable isotopes. ACS Earth Space Chem. 3, 1631–1639.
Yu, J.J., Zhang, Y.L., Ge, W.C., Yang, H., 2013a. Geochronology and geochemistry of the Late Cretaceous granitoids in the northern margin of the Sanjiang basin, NE China and its tectonic implications. Acta Petrol. Sin. 29 (2), 369–385 (in Chinese with English abstract).
Yu, J.J., Hou, X.G., Ge, W.C., Zhang, Y.L., Liu, J.C., 2013b. Magma mixing genesis of the early Permian Liulian pluton at the northeastern margin of the Jiamusi massif in NE China: evidences from petrography, geochronology and geochemistry. Acta Petrol. Sin. 29 (09), 2971–2986 (in Chinese with English abstract).
Yuan, L.L., Zhang, X.H., Xue, F.H., Liu, F.L., 2016. Juvenile crustal recycling in an accretionary orogen: Insights from contrasting Early Permian granites from central Inner Mongolia, North China. Lithos 264, 524–539.
Zhang, N., 2013. Late Paleozoic tectonic framework and evolution for the Dashizhai area Inner Mongolia, China. PhD. thesis, China University of Geosciences (Beijing), p. 162 pp..
Zhang, X.X., Gao, Y.F., Lei, S.H., 2018b. Geochronology and Geochemistry of the Early Permian A-Type Granite in the Hongol Area, Central Inner Mongolia: Petrogenesis and Tectonic Implications. Acta Geol. Sin. Engl. 92 (03), 988–1007.
Zhang, Y.M., Gu, X.X., Liu, R.P., Sun, X., Li, X.L., Zheng, L., 2017. Geology, geochronology and geochemistry of the Gaogangshan Mo deposit: A newly discovered Permo-Triassic collision-type Mo mineralization in the Lesser Xing'an Range, NE China. Ore Geol. Rev. 81, 672–688.
Zhang, Y.L., Guo, X.Q., Sun, L.X., Ma, S.X., Shi, L.Z., 2021. Detrital heavy minerals analysis of Early Permian Shoushangou Formation in the Xi Ujimqin, Inner Mongolia: Implications for provenance and tectonic setting. Acta Petrol. Et Mineral. 40 (6), 1155–1170 (in Chinese with English abstract).
Zhang, L., Jiang, S.Y., 2021. Early Permian continental arc magmatism in the Zhaojinggou area of the northern North China Craton: Implications for crust-mantle interactions during southward Paleo-Asian plate subduction. Lithos 390–391, 106110.
Zhang, L., Han, B.F., Zhu, Y.F., Xu, Z., Chen, J.F., Song, B., 2009. Geochronology, mineralogy, crystallization process and tectonic implications of the Shuangyashan monzogabbro in eastern Heilongjiang Province. Acta Petrol. Sin. 25 (3), 577–587 (in Chinese with English abstract).
Zhang, X.F., Wang, B.R., Zhang, H.C., Zou, Y., Feng, J.L., Cao, J., Teng, C., Liu, J.L., 2018a. The detrital zircon LA-ICP-MS U-Pb age of Early Permian Shoushangou Formation in Hanwula area of Xi Ujimqin Banner, Inner Mongolia, and its significance. Geological Bulletin of China 37 (5), 863–880 (in Chinese with English abstract).
Zhao, Z., Chi, X.G., Pan, S.Y., Liu, J.F., Sun, W., Hu, Z.C., 2010. Zircon U-Pb LA-ICP-MS dating of Carboniferous volcanic and its geological significance in the northwestern Lesser Xing'an Range. Acta Petrol. Sin. 26 (8), 2452–2464 (in Chinese with English abstract).
Zhao, P., Jahn, B.M., Xu, B., Liao, W., Wang, Y.Y., 2016. Geochemistry, geochronology and zircon Hf isotopic study of peralkaline-alkaline intrusions along the northern margin of the North China Craton and its tectonic implication for the southeastern Central Asian Orogenic Belt. Lithos 261, 92–108.
Zhao, L.L., Zhang, X.Z., 2011. Petrological and geochronological evidences of tectonic exhumation of Heilongjiang complex in the eastern part of Heilongjiang Province, China. Acta Petrol. Sin. 27 (4), 1227–1234 (in Chinese with English abstract).
Zhou, J.B., Wilde, S.A., 2013. The crustal accretion history and tectonic evolution of the NE China segment of the Central Asian Orogenic Belt. Gondwana Res. 23 (4), 1365–1377.
Zhou, J.B., Wilde, S.A., Zhao, G.C., Zhang, X.Z., Wang, H., Zeng, W.S., 2010. Was the easternmost segment of the Central Asian Orogenic Belt derived from Gondwana or Siberia: An intriguing dilemma? J. Geodyn. 50 (3–4), 300–317.
Zhou, J.B., Han, J., Zhao, G.C., Zhang, X.Z., Cao, J.L., Wang, B., Pei, S.H., 2015. The emplacement time of the Hegenshan ophiolite: Constraints from the unconformably overlying Paleozoic strata. Tectonophysics 662, 398–415.
Zhou, J.B., Pu, X.G., Hou, H.S., Han, W., Cao, J.L., Li, G.Y., 2018. The Mesozoic accretionary complex in NE China and its tectonic implications for the subduction of the Paleo-Pacific plate beneath the Eurasia. Acta Petrol. Sin. 34 (10), 2845–2856 (in Chinese with English abstract).
Zhou, H., Zhao, G.C., Han, Y.G., Zhang, D.H., Qian, L., Enkh-Orshikh, O., Zhao, Q., Pei, X.Z., 2021. The Late Carboniferous to Early Permian high silica magmatism in the southern Mongolia: Implications for tectonic evolution and continental growth. Gondwana Res. 97, 34–50.
Zhu, C.Y., Gao, R., Zhao, G.C., 2022. Permian to Cretaceous tectonic evolution of the Jiamusi and Songliao blocks in NE China: Transition from the closure of the Paleo-Asian Ocean to the subduction of the Paleo-Pacific Ocean. Gondwana Res. 103, 371–388.
Zorin, Y.A., 1999. Geodynamics of the western part of the Mongolia-Okhotsk collisional belt, Trans-Baikal region (Russia) and Mongolia. Tectonophysics 306, 33–56.